Preprints.org

Article

Not peer-reviewed version

The Halo Effect and Quantum Vortices. Not So Dark with Alena Tensor

Piotr Ogonowski *

Posted Date: 9 March 2026

doi: 10.20944/preprints202510.1554.v7

Keywords: unification; alena tensor; dark energy; dark matter; spin-vorticity coupling

Preprints.org is a free multidisciplinary platform providing preprint service that is dedicated to making early versions of research outputs permanently available and citable. Preprints posted at Preprints.org appear in Web of Science, Crossref, Google Scholar, Scilit, Europe PMC.

Copyright: This open access article is published under a Creative Commons CC BY 4.0 license, which permit the free download, distribution, and reuse, provided that the author and preprint are cited in any reuse.

Preprints.org (www.preprints.org) | NOT PEER-REVIEWED | Posted: 9 March 2026 doi:10.20944/preprints202510.1554.v7

Disclaimer/Publisher's Note: The statements, opinions, and data contained in all publications are solely those of the individual author(s) and contributor(s) and not of MDPI and/or the editor(s). MDPI and/or the editor(s) disclaim responsibility for any injury to people or property resulting from any ideas, methods, instructions, or products referred to in the content.

Article

The Halo Effect and Quantum Vortices. Not so Dark with Alena Tensor

Piotr Ogonowski

Kozminski University, Jagiellonska 57/59, 03-301 Warsaw, Poland; piotrogonowski@kozminski.edu.pl

Abstract

Alena Tensor is a recently discovered class of energy-momentum tensors that proposes a general equivalence of the curved path and geodesic for analyzed spacetimes which allows the analysis of physical systems in curvilinear (GR), classical and quantum descriptions. This paper demonstrates that extending the existing dust description to a form that provides a full matter energy-momentum tensor in GR, naturally leads to the development of a halo effect for continuum media. The resulting effective dark sector contributes to the gravitational energy-momentum tensor while remaining decoupled from gauge currents and visible matter. This approach predicts an inclination-dependent lensing signal and provides a phenomenological approximation of galaxy rotation curves for 104 objects from the SPARC catalog. Using a single galaxy-dependent parameter, the model yields weighted RMS residuals comparable to or smaller than those obtained with MOND or standard one-parameter halo models in about 80% of the analysed galaxies, while allowing further refinements related to anisotropy and energy flux. The same tensor structure admits a consistent flat spacetime formulation, allowing rotational effects to be incorporated into a quantum description, model quantum vortices and reproduce Mashhoon effect. This is illustrated by an effective quantum Lagrangian enabling the interpretation of mass generation as an emergent property of the phase-spin equilibrium and leading to a structural analogy and a set of stability conditions of quantum vortices consistent with Yukawa and Higgs-like mechanisms.

Keywords: unification; alena tensor; dark energy; dark matter; spin-vorticity coupling

1. Introduction

Research on the dark sector has been ongoing for many years [1] and there is still no theoretical consensus [2] or convincing experimental evidence regarding its nature [3]. We have not found dark matter signals for the WIMP models [4], axions/ALPs [5], SIDM [6], despite new experimental approaches [7], experiments in underground detectors, LZ experiments, XENON-nT [8] or SuperCDMS [9], and the latest observational data (e.g., "Hubble tension", ”Sigma-8 tension”) make the issue of the dark sector even more puzzling [10]. The dominant theoretical model is still ΛCDM with dark matter haloes [11], although alternative theories such as MOND/relativistic generalizations [12,13], dark photons [14], TeVeS/related constructions, f(R) [15], black holes [16], or the recently popular ”emergent/entropic gravity” [17] have achieved some success at selected scales. However, all these approaches experience ups and downs depending on the subsequent observational data [18].

There is also considered the possibility of hybrid models (e.g. a superfluid DM combining features of MOND and DM) [19], or even incorrect/weakened estimates of baryon masses and systematic errors in the M/L estimate [20], and the interaction of dark matter and energy [21] but so far this entire massive effort by the scientific community has not yielded a definitive conclusion. We have more certainty about dark energy because the universe is definitely expanding, and there are ample, multiple, independent confirmations, eg. from SN Ia, BAO, and CMB [11,22]. It is still uncertain whether the cosmological constant is indeed constant, although recent DESI (BAO) analyses indicate

© 2026 by the author(s). Distributed under a Creative Commons CC BY license.

Preprints.org (www.preprints.org) | NOT PEER-REVIEWED | Posted: 9 March 2026 doi:10.20944/preprints202510.1554.v7

the possibility of w(z) dynamics [23], and the Euclid mission is rapidly delivering high-quality weak lensing maps and surveys that will be crucial for measuring the dark energy equation of state [24]

The Alena Tensor is a relatively young field of research and has not had much relevance to the dark sector until now. Previous work has focused on developing a dual description for physical systems with matter and fields in which the metric tensor is not a feature of spacetime but only a method of describing it. Its aim was to provide a smooth transition between curvilinear description consistent with GR [25] and a flat (classical and quantum [26]) description for simple cases with dust [27], which was analyzed mainly for physical systems with electromagnetic fields [28]. This paper will demonstrate that extending the Alena Tensor to the general case yields results that provide possible representation of the spherical dark matter halo and provide an interpretation for the cosmological constant. This work, however, does not modify Einstein equations but modifies the matter sector through anisotropic rotational stresses. There will be also derived Noether tensor with Belinfante improvement and the quantum effective Lagrangian, which enables quantum description of vortices and ensures that the same energy-momentum tensor governs GR, flat-space dynamics, and quantization

In the first part of the paper, an introduction to the Alena Tensor model for dust will be presented, then this approach will be extended to the general form of the matter energy-momentum tensor and analyzed for quantum and GR description. The obtained GR equations will then be analyzed for their ability to describe the halo effect and lensing. The quantum description will also be analyzed in effective field-theoretic model and tested for its ability to describe elementary particles. The results will be discussed and shown to lead to the conclusions described in the abstract. The present work should be understood as a programmatic framework that establishes the core theoretical structure and explores several phenomenological consequences, rather than as a single-phenomenon model.

2. The Extended Alena Tensor

In this chapter, the conclusions reached so far regarding the Alena Tensor will be recalled, the notation will be introduced, and the reasoning from the previous articles will be generalized to all gauge fields and all forces acting in the physical system. The author uses the Einstein summation convention, metric signature $(+,-,-,-)$ and commonly used notations

2.1. Transforming curved path into geodesic for dust

As a first step, one may generalize the solution proposed in [27] in such a way that the forces resulting from all gauge fields are related to the metric tensor of curved spacetime

One may begin the reasoning by introducing tensor $F^{\mu\nu\alpha\beta}$ defined in terms of the gauge field tensors $\mathbb{F}_A^{\mu\nu}$ for each gauge group A, and the stress-energy tensor $\Upsilon^{\mu\nu}$ for such generalized field

$$F^{\mu\nu\alpha\beta} \equiv \sum_A \mathbb{F}_A^{\mu\nu} \otimes \mathbb{F}_A^{\alpha\beta}; \quad \Upsilon^{\mu\nu} \equiv F^{\mu\alpha\nu\beta} g_{\alpha\beta} - g^{\mu\nu} \frac{1}{4} F^{\alpha\gamma\beta\delta} g_{\alpha\beta} g_{\gamma\delta} \tag{1}$$

and denote the invariant of this field as p_Λ. Following reasoning from [27] let this field invariant be defined dually as follows

$$p_\Lambda \equiv \frac{1}{4} F^{\alpha\gamma\beta\delta} g_{\alpha\beta} g_{\gamma\delta} \equiv p_o \mathbb{k}^2 \quad ; \quad \mathbb{k} \equiv \mathbb{k}_{\mu\nu} g^{\mu\nu} \tag{2}$$

where p_o is certain constant (or simply invariant, independent of the metric) and where $\mathbb{k}^{\mu\nu}$, as raised in [26], in this approach is a metric tensor describing a curved spacetime in which all motion occurs along geodesics. By making variation on $-p_\Lambda$ with respect to metric $g_{\mu\nu}$ (Hilbert's method) one obtains the energy-momentum tensor of the field from (1) expressed dually as

$$\Upsilon^{\mu\nu} = p_\Lambda \left(\frac{4}{\mathbb{k}} \mathbb{k}^{\mu\nu} - g^{\mu\nu} \right) \tag{3}$$

© 2026 by the author(s). Distributed under a Creative Commons CC BY license.

Preprints.org (www.preprints.org) | NOT PEER-REVIEWED | Posted: 9 March 2026 doi:10.20944/preprints202510.1554.v7

Such approach, exactly as shown in [27], establishes a relationship between the field and the metric tensor $\mathbb{k}^{\mu\nu}$ and in the spacetime considered as described by the metric tensor $g^{\mu\nu} \rightarrow \mathbb{k}^{\mu\nu}$, one obtains $\mathbb{k} = 4$ what yields that in curvilinear description of the system, energy-momentum tensor of the field $\Upsilon^{\mu\nu}$ vanishes, maintaining continuity of function. As shown in previous articles, this causes the presence of a field in curved spacetime to manifest itself solely through curvature, which replaces the four-force densities in flat spacetime

In flat spacetime, one may assume that the equations of motion for the gauge fields A are satisfied, thus one obtains gauge four-currents $J^{\nu}_{A} \equiv D_{\mu}\mathbb{F}^{\mu\nu}_{A}$. Therefore, the total density of the Yang-Mills four-forces [29,30] f^{ν}_{YM} is

$$f^{\nu}_{YM} = \partial_{\mu}\Upsilon^{\mu\nu} = \sum_{A} J^{\alpha}_{A}\, \mathbb{F}^{\nu}_{A\alpha} \tag{4}$$

where the self-interactions of gauge fields in a non-Abelian theory are reducing. Then, following the reasoning presented in [27] one may define coefficient $\chi_m \equiv \frac{\varrho c^2}{p_\Lambda}$ where ϱ represents matter density and is associated with the translational current $\chi_m U^{\mu}$. In the Alena Tensor approach, the existence of matter is thus a manifestation of the existence of fields what ensures that without fields matter does not exist.

This allows one to define the Lagrangian $\mathcal{L}_{dust}$ and obtain from it the stress-energy tensor (Alena Tensor) for the system with dust $T^{\mu\nu}_{dust}$ by variation on the metric

$$\mathcal{L}_{dust} \equiv p_\Lambda(1-\chi_m) \quad \rightarrow \quad T^{\mu\nu}_{dust} \equiv \varrho U^{\mu}U^{\nu} - (1-\chi_m)\Upsilon^{\mu\nu} \tag{5}$$

In accordance with [28], assuming ϱ_o as rest mass density, four-momentum density is defined as $\varrho U^{\alpha} \equiv \varrho_o \gamma U^{\alpha}$ what takes into account motion and Lorentz contraction of the volume. Total four-force density acting on matter is therefore defined as

$$f^{\nu} \equiv \partial_{\mu}\varrho U^{\mu}U^{\nu} = \varrho U^{\mu}\partial_{\mu}U^{\nu} = \varrho\frac{dU^{\nu}}{d\tau}\,; \quad \partial_{\mu}\varrho U^{\mu} = 0 \tag{6}$$

As shown in [26], the above amendment introduces a natural property concerning curved spacetime, assuming that for dust, geodesic motion is expected

$$\partial_{\alpha}\varrho U^{\alpha} = 0 \rightarrow U^{\alpha}{}_{,\alpha} = -\frac{d\gamma}{dt} \rightarrow U^{\alpha}{}_{;\alpha} = 0 \tag{7}$$

$$U^{\alpha}U^{\beta}{}_{;\alpha} = 0 \rightarrow \frac{D\,U^{\beta}}{D\,\tau} = 0\,;\ \left(\varrho\, U^{\alpha}U^{\beta}\right)_{;\alpha} = 0 \tag{8}$$

Next, it can be calculated that in flat spacetime the four-divergence of the tensor $T^{\mu\nu}_{dust}$ can be interpreted as the density of the four-forces acting on matter f^{ν} reduced by the density of the field-related four-forces

$$f^{\nu}_{field} \equiv \partial_{\mu}\left[(1-\chi_m)\Upsilon^{\mu\nu}\right] = (1-\chi_m)f^{\nu}_{YM} + f^{\nu}_{gr} \tag{9}$$

$$f^{\nu}_{gr} \equiv \Upsilon^{\mu\nu}\partial_{\mu}(1-\chi_m) = -\Upsilon^{\mu\nu}\partial_{\mu}\chi_m = \varrho\left(\frac{d\phi}{d\tau}U^{\nu} - c^2\partial^{\nu}\phi\right) \tag{10}$$

As shown in [26], the f^{ν}_{gr} can be associated with the existence of gravity in the system, while the possibility of reproducing the GR geodetic movement by equations of motion in flat spacetime based on potential ϕ has been already confirmed, e.g. in [31]. The four-force density $f^{\nu}_{rr} \equiv \chi_m f_{YM}$ behaves as a radiation-reaction force, reducing the value of forces due to the field and upholding the conservation of energy, ensuring that the increasing energy density associated with matter ϱc^2 does not exceed the total energy density p_Λ available in the system

$$0 = \partial_{\mu}T^{\mu\nu}_{dust} = f^{\nu} - f^{\nu}_{field} = f^{\nu} - f^{\nu}_{YM} - f^{\nu}_{gr} + f^{\nu}_{rr} \tag{11}$$

© 2026 by the author(s). Distributed under a Creative Commons CC BY license.

Preprints.org (www.preprints.org) | NOT PEER-REVIEWED | Posted: 9 March 2026 doi:10.20944/preprints202510.1554.v7

where $\lim_{\chi_m \to 1} f^{\nu}_{field} = 0$.

Presented approach, as shown in [27] allows one to interpret the existence of $\mathrm{Y}^{\mu\nu}$ as a perturbation of the metric on the flat Minkowski background, thus $\mathrm{Y}^{\mu\nu}$ can be treated as a potential for the Weyl tensor. This also indicates the ansatz for the Kerr-Schild type metrics for curved spacetime

$$\mathbb{k}^{\mu\nu} \equiv \sum_i c_i l_i^{\mu} l_i^{\nu} + \frac{\mathbb{k}}{4}\eta^{\mu\nu}\,; \quad 0 = \eta_{\mu\nu} l_i^{\mu} l_i^{\nu} \tag{12}$$

where l_i^{μ} are null vectors and c_i are related coefficients

In the next section, the above model will be expanded to include rotation-related components, which will prove crucial for describing dark sector phenomena and allow to obtain a description that agrees with the observational results.

2.2. Rotational energy

It can be noticed that the radiation reaction force should take into account the total energy associated with the body, so in addition to the energy associated with the translational motion, it seems necessary to take into account the rotational energy

One may thus introduce a projector $\Delta^{\mu\nu}$, flow vorticity tensor $\omega^{\mu\nu}$, positive coefficient χ_ω equal to the rotational energy $\mathcal{E}_{rot}$ up to p_Λ (thus $\mathcal{E}_{rot} \equiv p_\Lambda \chi_\omega$) and some metric independent auxiliary α with the dimension of the square of time

$$\Delta^{\mu}{}_{\nu} \equiv g^{\mu}{}_{\nu} - \frac{1}{c^2} U^{\mu} U_{\nu}\,; \quad \omega_{\mu\nu} \equiv \Delta_{\mu}{}^{\alpha}\Delta_{\nu}{}^{\beta}\nabla_{[\alpha}U_{\beta]}\,; \quad \chi_\omega \equiv \frac{\alpha}{2}\,\omega^{\mu\nu}\omega_{\mu\nu} \tag{13}$$

Defining Lagrangian density $\mathcal{L}_T$ for the whole system and tensor $B^{\lambda\mu\nu}$ to describe emerging boundary terms

$$\mathcal{L}_T = p_\Lambda(1 - \chi_\omega - \chi_m)\,; \quad B^{\lambda\mu\nu} \equiv p_\Lambda \alpha \left(U^{\lambda}\omega^{\mu\nu} - U^{(\mu}\omega^{\nu)\lambda} \right) \tag{14}$$

and introducing $\Xi^{\mu\nu}$ tensor related to rotational properties of the system

$$-\Xi^{\mu\nu} \equiv \alpha\, p_\Lambda \left(\omega^{\mu\gamma}\omega^{\nu}{}_{\gamma} - \frac{1}{2}\Delta^{\mu\nu}\omega^{\alpha\beta}\omega_{\alpha\beta} \right) + \nabla_\lambda B^{\lambda(\mu\nu)} \tag{15}$$

one obtains Alena Tensor $T^{\mu\nu}$ for the system derived with help of variational method on $\mathcal{L}_T$ in the form

$$T^{\mu\nu} = \varrho U^{\mu} U^{\nu} - \Xi^{\mu\nu} - (1 - \chi_\omega - \chi_m)\mathrm{Y}^{\mu\nu}\,; \quad T^{\mu\nu} g_{\mu\nu} = \varrho c^2 - \mathcal{E}_{rot} \tag{16}$$

Considering description in curved spacetime, described by the metric tensor $\mathbb{k}^{\mu\nu}$, the field tensor $\mathrm{Y}^{\mu\nu}$ vanishes, the system tensor reduces to the form $T^{\mu\nu}_{matt} \equiv \varrho U^{\mu} U^{\nu} - \Xi^{\mu\nu}$ and its vanishing four-divergence means that any deviations from the geodesic motion with $a^{\mu} \equiv U^{\nu}\nabla_{\nu}U^{\mu}$ are compensated by rotation related forces. Using the standard kinematic decomposition one may calculate

$$\varepsilon \equiv \frac{1}{c^2} T^{\mu\nu}_{matt} U_{\mu} U_{\nu} = \varrho c^2 + 2\mathcal{E}_{rot} \tag{17}$$

$$T^{\mu\nu}_{matt} U_{\nu} = \left(\varrho c^2 + 2\mathcal{E}_{rot} \right) U^{\mu} - \alpha\, p_\Lambda \left(a_\nu \omega^{\nu\mu} + \frac{c^2}{2}\Delta^{\mu}{}_{\nu}\nabla_\lambda \omega^{\lambda\nu} \right) \tag{18}$$

where the element in brackets in last equation represents in fact the purely spatial vorticity divergence. Assuming the classical definition of the energy flux q^{α} one also gets

$$q^{\alpha} \equiv \frac{1}{c^2}\Delta^{\alpha}{}_{\mu} T^{\mu\nu}_{matt} U_{\nu} = -\alpha\, p_\Lambda \left(a_\nu \omega^{\nu\alpha} + \frac{c^2}{2}\Delta^{\alpha}{}_{\nu}\nabla_\lambda \omega^{\lambda\nu} \right) \tag{19}$$

© 2026 by the author(s). Distributed under a Creative Commons CC BY license.

Preprints.org (www.preprints.org) | NOT PEER-REVIEWED | Posted: 9 March 2026 doi:10.20944/preprints202510.1554.v7

Introducing classical shear tensor $\sigma^{\mu\nu}$ and effective vortex stress tensor $\tau^{\mu\nu}$ as

$$\sigma^{\mu\nu} \equiv \Delta^{\mu\alpha}\Delta^{\nu\beta}\nabla_{(\alpha}U_{\beta)} - \frac{1}{3}\nabla_{\alpha}U^{\alpha}\Delta^{\mu\nu}\,;\ \tau^{\mu\nu} \equiv \frac{p_{\Lambda}\alpha}{2}\Big(\sigma^{\mu}{}_{\lambda}\omega^{\nu\lambda} + \sigma^{\nu}{}_{\lambda}\omega^{\mu\lambda}\Big) \tag{20}$$

one may thus rewrite $T^{\mu\nu}_{matt}$ in curved spacetime as

$$T^{\mu\nu}_{matt} = \frac{\varepsilon}{c^2}U^{\mu}U^{\nu} + \frac{1}{c^2}(U^{\mu}q^{\nu} + U^{\nu}q^{\mu}) - \mathcal{E}_{rot}\Delta^{\mu\nu} - \tau^{\mu\nu} \tag{21}$$

One may notice that the system has a built-in anisotropic stress described by $\tau^{\mu\nu}$, but its source is not viscosity, but the coupling between shear and vorticity (between flow deformation and local spin angular momentum)

Considered in flat spacetime such approach introduces additional four-force density f^{ν}_{Ξ} acting on matter and also changes f^{ν}_{gr} and the radiation reaction f^{ν}_{rr} to the form

$$f^{\nu}_{\Xi} \equiv \partial_{\mu}\Xi^{\mu\nu}\,;\ f^{\nu}_{rr} = (\chi_m + \chi_\omega)f^{\nu}_{YM}\,;\ f^{\nu}_{gr} = \Upsilon^{\mu\nu}\partial_{\mu}(1 - \chi_\omega - \chi_m) \tag{22}$$

One may now consider the impact of the above expansion of the Alena Tensor on quantum equations and GR equations

2.2.1. Noether tensor and quantum interpretation

One may consider $\mathcal{L}_T$ from (14) in flat spacetime. The canonical Noether energy-momentum tensor associated with translations is

$$T^{\mu\nu}_{\text{can}} \equiv \sum_{\phi}\frac{\partial\mathcal{L}_T}{\partial(\partial_{\mu}\phi)}\,\partial^{\nu}\phi - \eta^{\mu\nu}\,\mathcal{L}_T \quad ; \quad \partial_{\mu}T^{\mu\nu}_{\text{can}} = 0\ (\text{on}-\text{shell}) \tag{23}$$

where the sum runs over all dynamical fields ϕ (here: U_α and gauge fields $\mathbb{A}_{\alpha A}$). Lorentz invariance implies conservation of the total angular momentum current $J^{\lambda\mu\nu}$ as

$$J^{\lambda\mu\nu} \equiv x^{\mu}T^{\lambda\nu}_{\text{can}} - x^{\nu}T^{\lambda\mu}_{\text{can}} + S^{\lambda\mu\nu} \quad ; \quad \partial_{\lambda}J^{\lambda\mu\nu} = 0 \tag{24}$$

with the spin current $S^{\lambda\mu\nu}$ written by the generators of Lorentz transformations acting on the space of field components marked as $\Sigma^{\mu\nu}$

$$S^{\lambda\mu\nu} \equiv \sum_{\phi}\frac{\partial\mathcal{L}_T}{\partial(\partial_{\lambda}\phi)}\,(\Sigma^{\mu\nu}\phi) \tag{25}$$

Substituting the explicit expressions for the spin current given in (24) together with the canonical momenta defined below, yields the explicit form of the Belinfante superpotential $Q^{\lambda\mu\nu}$ in terms of the velocity field U^{α} and the gauge field tensors $F^{\mu\nu}_{A}$. In this way the symmetrisation procedure leading to the Belinfante tensor $T^{\mu\nu}_{B}$ is completely determined by the field content of the Lagrangian. For a Lorentz vector field V_ρ one has $(\Sigma^{\mu\nu}V)_\rho = \eta^{\mu}{}_{\rho}V^{\nu} - \eta^{\nu}{}_{\rho}V^{\mu}$, hence in particular

$$S^{\lambda\mu\nu}_{U} = \Pi^{\lambda\mu}(U)\,U^{\nu} - \Pi^{\lambda\nu}(U)\,U^{\mu}\,;\ S^{\lambda\mu\nu}_{\text{gauge}} = \sum_{A}\Big(\Pi^{\lambda A\mu}(A)\,\mathbb{A}^{\nu}_{A} - \Pi^{\lambda A\nu}(A)\,\mathbb{A}^{\mu}_{A}\Big) \tag{26}$$

and $S^{\lambda\mu\nu} = S^{\lambda\mu\nu}_{U} + S^{\lambda\mu\nu}_{\text{gauge}}$. One may thus define the Belinfante superpotential $Q^{\lambda\mu\nu}$ as in [29] which is antisymmetric in the first two indices $Q^{\lambda\mu\nu} = -Q^{\mu\lambda\nu}$, and the Belinfante tensor $T^{\mu\nu}_{B}$ as

$$Q^{\lambda\mu\nu} \equiv \frac{1}{2}\Big(S^{\mu\lambda\nu} + S^{\nu\lambda\mu} - S^{\lambda\mu\nu}\Big) \quad ; \quad T^{\mu\nu}_{B} \equiv T^{\mu\nu}_{\text{can}} + \partial_{\lambda}Q^{\lambda\mu\nu} \tag{27}$$

© 2026 by the author(s). Distributed under a Creative Commons CC BY license.

Preprints.org (www.preprints.org) | NOT PEER-REVIEWED | Posted: 9 March 2026 doi:10.20944/preprints202510.1554.v7

Since partial derivatives commute in flat spacetime and $Q^{\lambda\mu\nu}$ is antisymmetric in (λ,μ), therefore $\partial_\mu\partial_\lambda Q^{\lambda\mu\nu}=0$ and thus $\partial_\mu T_B^{\mu\nu}=0$ on-shell. Using (24) and (27) one gets the standard identity

$$T^{\mu\nu}_{\rm can}-T^{\nu\mu}_{\rm can}=-\partial_\lambda S^{\lambda\mu\nu}\quad\rightarrow\quad T_B^{\mu\nu}=T_B^{\nu\mu} \tag{28}$$

For the U-sector the momentum conjugate to $\partial_\mu U_\alpha$ is

$$\Pi^{\mu\alpha}(U)\equiv\frac{\partial\mathcal{L}_T}{\partial(\partial_\mu U_\alpha)}=-\alpha p_\Lambda\,\omega^{\mu\alpha} \tag{29}$$

For the gauge sector, using definition of p_Λ from (2), one finds

$$\Pi^{\mu A}{}_{\alpha}(A)\equiv\frac{\partial\mathcal{L}_T}{\partial(\partial_\mu \mathbb{A}^\alpha_A)}=(1-\chi_\omega)\,\mathbb{F}^\mu_{A\alpha} \tag{30}$$

since the mass term $p_\Lambda\chi_m=\varrho c^2$ does not depend on $\partial_\mu\mathbb{A}^\alpha_A$

For a Poincaré-invariant theory in flat spacetime one has the Rosenfeld-Belinfante identity $T^{\mu\nu}=T_B^{\mu\nu}+\partial_\lambda\partial_\rho\,Y^{\lambda\rho\mu\nu}$, where $\partial_\lambda\partial_\rho\,Y^{\lambda\rho\mu\nu}$ is an identically conserved (pure-improvement) term. In above, the physical (symmetric, conserved) energy-momentum tensor $T^{\mu\nu}$ is Hilbert tensor from (16). Upon quantization, $T^{\mu\nu}$ is promoted to an operator and $\varrho c^2=\chi_m\,p_\Lambda$ admits a natural interpretation as $mc^2\bar\psi\psi$.

This also yields that in the quantum theory the four-velocity field U^μ is identified with the hydrodynamic limit of the Dirac current, $U^\mu=c\,\langle\bar\psi\gamma^\mu\psi\rangle/\sqrt{\langle\bar\psi\gamma^\nu\psi\rangle\langle\bar\psi\gamma_\nu\psi\rangle}$, rendering χ_ω a composite quantity determined by fermionic correlators. For a Dirac field coupled to gauge fields via $D_\mu=\partial_\mu-i\sum_A g_A\,\mathbb{A}_{\mu A}\,T_A$, one obtains in flat spacetime Lagrangian $\mathcal{L}_Q$ and the standard symmetric form

$$T^{\mu\nu} = \frac{i\hbar c}{4}\,\bar\psi\,\gamma^{(\mu}\overleftrightarrow{D}^{\nu)}\psi-\Xi^{\mu\nu}-(1-\chi_\omega-\chi_m)\,\mathrm{Y}^{\mu\nu} \tag{31}$$

$$\mathcal{L}_Q \equiv \frac{i\hbar c}{2}\,\bar\psi\,\gamma^\mu\overleftrightarrow{D}_\mu\psi+(1-\chi_\omega-\chi_m)p_\Lambda \tag{32}$$

where $\overleftrightarrow{D}$ denotes the two-way covariant derivative. The rotational sector described by $\Xi^{\mu\nu}$ and the vorticity-dependent screening of p_Λ provide an effective dark sector. It contributes to the gravitational energy-momentum tensor while remaining non-interacting with gauge currents and visible matter. As a consequence, the effective dark sector gravitates universally but does not participate in nongravitational interactions, which implies a natural dynamical separation from baryonic matter in systems undergoing mergers or collisions. This separation follows directly from the structure of the energy-momentum tensor and does not require additional fields, modified gravity, or ad hoc interaction terms

2.2.2. General Relativity Interpretation

One may now repeat the reasoning from [27] and define the generalized Ricci and Einstein tensors, where the˜sign indicates normalization with the constant $\kappa/2=\frac{4\pi G}{c^4}$, and additional tensor $\Theta^{\mu\nu}$ as

$$\tilde R^{\mu\nu} \equiv 2T^{\mu\nu}_{matt}+2\chi_\omega\mathrm{Y}^{\mu\nu}+\Big(p_\Lambda+\mathcal{E}_{rot}-\varrho c^2\Big)g^{\mu\nu} \tag{33}$$

$$\tilde R \equiv \tilde R^{\mu\nu}\,g_{\mu\nu}=4p_\Lambda+2\mathcal{E}_{rot}-2\varrho c^2 \tag{34}$$

$$\tilde G^{\mu\nu} \equiv \tilde R^{\mu\nu}-\frac{\tilde R}{2}\frac{4}{\mathbb{k}}\mathbb{k}^{\mu\nu}=\tilde R^{\mu\nu}-\frac{\tilde R}{2}g^{\mu\nu}-\frac{\tilde R}{2p_\Lambda}\mathrm{Y}^{\mu\nu}=2T^{\mu\nu}_{matt}-(2-\chi_m-\chi_\omega)\mathrm{Y}^{\mu\nu}-p_\Lambda g^{\mu\nu} \tag{35}$$

$$\Theta^{\mu\nu} \equiv -(\chi_m+\chi_\omega)\,\mathrm{Y}^{\mu\nu}\quad\rightarrow\quad\tilde G^{\mu\nu}+p_\Lambda\,g^{\mu\nu}=2T^{\mu\nu}+\Theta^{\mu\nu} \tag{36}$$

© 2026 by the author(s). Distributed under a Creative Commons CC BY license.

Preprints.org (www.preprints.org) | NOT PEER-REVIEWED | Posted: 9 March 2026 doi:10.20944/preprints202510.1554.v7

where the last equality holds in any considered spacetime and for $G^{\mu\nu} = \frac{\kappa}{2}\tilde{G}^{\mu\nu}$, $\Lambda = \frac{\kappa}{2}p_\Lambda$ becomes the classical GR equation in curved spacetime (in curved spacetime $\Upsilon^{\mu\nu}$ and $\Theta^{\mu\nu}$ vanish)

The Lagrangian $\mathcal{L}_\Theta$ for $\Theta^{\mu\nu}$ may be obtained the same way as in [27] with the use of the interpolating path method $g^{\mu\nu}(\lambda) = (1-\lambda)\mathbb{k}^{\mu\nu} + \lambda g^{\mu\nu}$. Using this method one obtains

$$\sqrt{-g}\,\mathcal{L}_\Theta \equiv \frac{1}{2}\int_0^1 d\lambda\,\sqrt{-g(\lambda)}\,\Theta_{\mu\nu}\left[g^{\mu\nu}(\lambda)\right]\,\partial_\lambda g^{\mu\nu}(\lambda) \tag{37}$$

Since the variation of the functional is located on the boundary $\lambda = 1$, thus $\Theta_{\mu\nu} = \frac{2}{\sqrt{-g}}\frac{\delta(\sqrt{-g}\mathcal{L}_\Theta)}{\delta g^{\mu\nu}}$.

In the last equation of (36) considered in curved spacetime ($g^{\mu\nu} \to \mathbb{k}^{\mu\nu}$) field invariant p_Λ acts as double the vacuum energy density (vacuum pressure). This equation may be derived from the Lagrangian density $\mathcal{L}_G$ in the form

$$\mathcal{L}_G \equiv 2\mathcal{L}_T + \mathcal{L}_\Theta = \mathcal{L}_{matt} + \frac{1}{2}\tilde{R} - 2\mathcal{E}_{rot}\,;\ \mathcal{L}_{matt} \equiv \mathcal{L}_\Theta - p_\Lambda(\chi_m + \chi_\omega) \tag{38}$$

where the variation by Hilbert's method on $\mathcal{L}_{matt}$ gives $T^{\mu\nu}_{matt} \equiv \varrho U^\mu U^\nu - \Xi^{\mu\nu}$.

The equation (35) considered in curved spacetime simplifies to $\tilde{G}^{\mu\nu} = \tilde{R}^{\mu\nu} - \frac{\tilde{R}}{2}g^{\mu\nu}$ where $\Upsilon^{\mu\nu}$ and thus also $\Theta^{\mu\nu}$ vanishes. It is also worth noting that in flat spacetime the generalized Einstein tensor is associated with the four-divergence of $\Theta^{\mu\nu}$

$$\partial_\mu\tilde{G}^{\mu\nu} = \partial_\mu\Theta^{\mu\nu} = f^\nu_{gr} - f^\nu_{rr} \tag{39}$$

so the curvature it describes in curved spacetime replaces this four-force density, where f^ν_{gr} is related to gravity and f^ν_{rr} is the density of radiation-reaction four-force. The presence of the radiation-reaction force has already been discussed in previous works [25], and it now prevents the matter energy and rotational energy from increasing beyond the maximum energy density p_Λ available in the system.

It is worth noting that internal energy density and rotational energy, essentially exhaust the possible forms of energy that can be attributed to material bodies (other forms of energy, e.g., chemical energy, can be treated as their components) which could be present in the radiation reaction force. This means that the model proposed here seems complete (with the possible extension of α to a tensor form for more complex systems) and should allow for reproducing the results obtained from GR, as well as reproducing observational results that are inconsistent (such as the dark sector) with currently used interpretation of GR.

Alena Tensor approach therefore allows one to look at Einstein's equations in a new light and analyze the possibilities of explaining the dark sector in a consistent mathematical framework that allows analysis in both flat and curved spacetime. Importantly, it is also possible to analyze the system using a quantum approach (in the description for flat spacetime) and to use standard tools of continuum mechanics for continuous media in flat and curved spacetime, where the description of the behavior of matter has been separated into effects related to fundamental interactions f^ν_{YM}, gravity and radiation reaction $f^\nu_{gr} - f^\nu_{rr}$, and forces related to the distribution of matter f^ν_Ξ.

3. Results

The following section will present the results of applying the Alena Tensor model both to cosmological objects and to describe quantum vortices

© 2026 by the author(s). Distributed under a Creative Commons CC BY license.

Preprints.org (www.preprints.org) | NOT PEER-REVIEWED | Posted: 9 March 2026 doi:10.20944/preprints202510.1554.v7

3.1. The halo effect

The obtained results de facto means that Alena Tensor ensures correct operation of the standard continuum mechanics equations and GR equations (Euler equations, EOS, TOV, first integrals for rotating stars, etc.), with assumption that the energy density used in them is $\varepsilon = \varrho c^2 + 2\mathcal{E}_{rot}$ and pressure is equal to $\mathcal{E}_{rot}$. In the next steps, this approach will be analyzed to show that it leads to consistency with the observational data

It's worth starting with a simple approximation. Denoting u_{rot} as rotational velocity and assuming

$$p_\Lambda \alpha = \frac{1}{c^2\kappa}\,; \quad \varrho_{rot} \equiv \frac{2\mathcal{E}_{rot}}{c^2} = \frac{\omega^{\alpha\beta}\omega_{\alpha\beta}}{8\pi G} \quad \to \quad \lim_{r\to\infty} \varrho_{rot} = \frac{u_{rot}^2}{4\pi G r^2} \tag{40}$$

one may notice that $p_\Lambda \alpha$ in (15) plays the role of the density of the moment of inertia, while ϱ_{rot} increases the body's effective mass within its own frame. This would allow to consider galaxies as continuous media, where the effective mass M_{eff} and its density ϱ_{eff} responsible for gravity $\varrho_{eff} \equiv \frac{\varepsilon}{c^2} = \varrho + \varrho_{rot}$ from (17) increases with the galactic disk size and angular velocity, causing the halo effect

For far regions, denoting M_b as baryonic mass, for spherical symmetry one obtains from Poisson's equation simple linear ODE in the Newtonian limit. In the far regions it could determine a constant rotation speed and might be used to measure of deviation from the vacuum solution.

Vacuum solution $\left(T^{\mu\nu}_{matt} = 0\right)$ in curved spacetime from (34) and (16) yields

$$\tilde{R} \;=\; 4p_\Lambda \quad \to \quad \varrho c^2 = \mathcal{E}_{rot} = 0 \tag{41}$$

This means that Keplerian profiles are still possible for systems that can be approximated by the vacuum solution

Going into a more detailed analysis, one may analyse axisymmetric, stationary metric

$$ds^2 \;=\; N^2c^2dt^2 - A^2\left(dr^2 + r^2d\theta^2\right) - B^2r^2\sin^2\theta(d\phi - \omega dt)^2 \tag{42}$$

which in general case implies the existence of two Killing vectors $\xi^\mu = (\partial_t)^\mu$, $\eta^\mu = (\partial_\phi)^\mu$. For the energy-momentum tensor in the hydrodynamic distribution as in (21), one can therefore define Killing currents $J^\mu_E \equiv T^{\mu\nu}\xi_\nu = T^\mu_t$ and $J^\mu_L \equiv T^{\mu\nu}\eta_\nu = T^\mu_\phi$ which satisfy $0 = \nabla_\mu J^\mu_E = \nabla_\mu J^\mu_L$. From the algebraic identity (for any Killing vector K^μ)

$$J^\mu[K] \equiv T^{\mu\nu}K_\nu = \frac{\varepsilon}{c^2}U^\mu(U\cdot K) + \frac{1}{c^2}\left[U^\mu(q\cdot K) + (U\cdot K)\,q^\mu\right] - \mathcal{E}_{\rm rot}\,\Delta^{\mu\nu}K_\nu - \tau^{\mu\nu}K_\nu \tag{43}$$

one obtains, in particular, for the angular momentum ($K = \eta$) the form of a mixed component

$$T^\mu{}_\phi = \frac{\varepsilon + \mathcal{E}_{\rm rot}}{c^2}\,U^\mu U_\phi + \frac{1}{c^2}\left(U^\mu q_\phi + q^\mu U_\phi\right) - \tau^\mu{}_\phi - \;\mathcal{E}_{\rm rot}\,\delta^\mu{}_\phi \tag{44}$$

Consequently, the transport components (radial and meridional) have the form

$$T^r{}_\phi \;=\; \frac{\varepsilon + \mathcal{E}_{\rm rot}}{c^2}\,U^r U_\phi + \frac{1}{c^2}\left(U^r q_\phi + q^r U_\phi\right) - \tau^r{}_\phi \tag{45}$$

$$T^\theta{}_\phi \;=\; \frac{\varepsilon + \mathcal{E}_{\rm rot}}{c^2}\,U^\theta U_\phi + \frac{1}{c^2}\left(U^\theta q_\phi + q^\theta U_\phi\right) - \tau^\theta{}_\phi \tag{46}$$

For circular flow $0 = U^r = U^\theta$, the convective terms from U^r, U^θ disappear, so the currents reduce to

$$T^r{}_\phi = \frac{q^r U_\phi}{c^2} - \tau^r{}_\phi \quad ; \quad T^\theta_\phi = \frac{q^\theta U_\phi}{c^2} - \tau^\theta{}_\phi \tag{47}$$

© 2026 by the author(s). Distributed under a Creative Commons CC BY license.

Preprints.org (www.preprints.org) | NOT PEER-REVIEWED | Posted: 9 March 2026 doi:10.20944/preprints202510.1554.v7

This means that in the stationary and axisymmetric regime, the "halo" can be interpreted not as additional mass, but as a result of angular momentum transport via the energy flux q^μ and anisotropic stresses $\tau^\mu{}_\nu$, which generate non-zero fluxes $T^r{}_\phi$ and/or $T^\theta{}_\phi$

One may also consider a simplified analysis based on an ideal-fluid approximation $\left(\tau^{\mu\nu}=0,\, U^{(\mu}q^{\nu)}=0\right)$, leaving only the contribution of the rotational current discussed above, which appears in the form of an effective pressure $p \equiv \mathcal{E}_{\rm rot}$. In this case the energy-momentum tensor reduces to

$$T^{\mu\nu}_{\rm ideal} \equiv \left(\varrho + \frac{2p}{c^2}\right)U^\mu U^\nu - p\Delta^{\mu\nu} \tag{48}$$

Analyzing Euler's energy and momentum equations for $\nabla_\mu T^{\mu\nu}_{\rm ideal} = 0$, one finds that the velocity measured by locally non-rotating observers is not geodesic. On the equatorial plane it takes the form

$$\frac{u^2_{\rm ZAMO}}{c^2} = \frac{(Br)^2}{N^2}\left(\frac{d\phi}{dt}-\omega\right)^2 = r\,\partial_r \ln N + \gamma_p^2 - 1 \quad ; \quad \gamma_p^2 \equiv 1 - r\frac{p'}{\varrho c^2 + 3p} \tag{49}$$

Here $u_{\rm ZAMO}$ denotes the velocity measured by locally non-rotating observers (ZAMO), i.e. observers with zero angular momentum with respect to infinity in a stationary axisymmetric spacetime. Such observers follow worldlines orthogonal to hypersurfaces of constant coordinate time and therefore provide the natural local inertial frame for rotating systems. The ZAMO construction and the corresponding velocity definition are standard in relativistic rotating flows [32–34]. The resulting expression therefore corresponds to the velocity measured in the locally non-rotating frame associated with the metric introduced above and represents the physically relevant velocity entering the Euler equations for stationary rotating configurations

One may therefore define the pressure contribution as

$$\kappa p \equiv \frac{u^2_{\rm ZAMO}}{r^2c^2} \;\rightarrow\; \frac{dM_{\rm eff}}{dr} = 4\pi r^2 \varrho(r) + \frac{u^2_{\rm ZAMO}}{G} \;\rightarrow\; \frac{d}{dr}u^2_{\rm ZAMO} = 4\pi G r\,\varrho(r) \tag{50}$$

In this picture the velocity increase depends solely on the baryonic mass distribution, while the flattening of the rotation curve at large radii is maintained by the rotational energy component. This behavior precisely mimics the phenomenology usually attributed to a dark matter halo. The introduction of q^μ and $\tau^{\mu\nu}$ into a system can be approximated by defining parameter $\chi(r)$ changing original p used for isotropic model. Assuming $p_r \equiv \beta_r p$ and $p_\theta \equiv \beta_\theta p$ one may introduce

$$p_\phi \equiv p \;\rightarrow\; \chi = \beta_r + \beta_\theta\,;\, 3p_\chi \rightarrow (1+\chi)p\,;\, 2p \rightarrow \chi p \tag{51}$$

The constant χ analysis should be regarded as an illustrative limit rather than a physical assumption and is comparable in quality to standard one-parameter halo models. In practice, even a constant χ should be sufficient for analyzing the fit of galaxy rotation curves. Using a constant χ also provides a simpler ODE and the ability to quickly perform preliminary fits of χ to observational data for large amounts of data.

$$\begin{aligned} \frac{dM_{eff}}{dr} &= 4\pi r^2\varrho(r) + \frac{\chi}{2}\frac{u^2_{ZAMO}}{G} \quad \rightarrow \\ \frac{d}{dr}u^2_{ZAMO} &= 4\pi G r\,\varrho(r) + \left(\frac{\chi}{2}-1\right)\frac{u^2_{ZAMO}}{r}\,; \quad \lim_{\varrho\to 0} u^2_{ZAMO} \propto r^{\frac{\chi}{2}-1} \end{aligned} \tag{52}$$

On the Fig. 1 below, one may find the expected course of the rotation curves depending on the assumed constant χ.

Figure 1. Approx. rotation curves in Alena Tensor model

© 2026 by the author(s). Distributed under a Creative Commons CC BY license.

Preprints.org (www.preprints.org) | NOT PEER-REVIEWED | Posted: 9 March 2026 doi:10.20944/preprints202510.1554.v7

The calculations used an averaged Hernquist bulge baryon model ϱ_{bulge} and a "spherical proxy" of the exponential disk ϱ_{disc}

$$\varrho_{bulge} = \frac{M_{bulge}}{2\pi}\frac{a}{r(r+a)^3} \quad ; \quad M_{bulge} = 10^{10}M_{\odot} \quad ; \quad a = 1kpc \tag{53}$$

$$\varrho_{disc} = \frac{M_{disc}}{4\pi R_d^2}\frac{e^{-r/R_d}}{r} \quad ; \quad R_d = 3kpc \tag{54}$$

with total baryon density $\varrho_b(r) = \varrho_{bulge} + \varrho_{disc}$, standard G value, anisotropy and energy stream simulated by constant χ. As can be seen from the graph, the increasing anisotropy towards the outskirts of the galaxy $\chi(r = 0) = 0$; $\lim_{r\to\infty}\chi(r) = const$ would allow the graph to align with the expected curve shapes for spiral galaxies

As it appears, a constant value of χ allows one to tune the rotation velocity distribution for a significant subset of galaxies, providing a first overview of the method and a starting point for further analysis using a radial function $\chi(r)$. The results of fitting a constant χ to approximately 100 galaxies from the SPARC catalog [35] are presented in C

In this numerical exploration the baryonic density entering eq. (52) is reconstructed from the baryonic rotation curve $V_{\rm bar}(r)$ using a spherical inversion routine (implemented in the supplementary Mathematica script as `rhoFromVbar`). This procedure should be understood as a phenomenological spherical proxy for the baryonic mass distribution rather than a physical reconstruction of the disk potential. Its purpose is purely computational, and allows the differential equation (52) to be integrated directly from the observed baryonic rotation curves without introducing an explicit disk-potential decomposition or solving the Poisson equation numerically. Consequently, the present analysis should be interpreted as an exploratory test of the scaling behaviour predicted by the model rather than as a detailed reconstruction of the gravitational field of galactic disks

Importantly, the additional gravitational contribution predicted in the Alena Tensor framework does not depend on the geometrical orientation of the baryonic disk itself. In this model the extra source term arises from the rotational invariant $\omega_{\mu\nu}\omega^{\mu\nu}$ entering the energy-momentum tensor through the rotational energy density $\mathcal{E}_{\rm rot}$. As a scalar invariant of the flow, this quantity depends primarily on the magnitude of the rotational motion rather than on the planar geometry of the disk. At large radii the associated gravitational response can therefore appear approximately isotropic even when the baryonic rotation is confined to a disk. Cosmological simulations of galaxy formation also show that angular-momentum transport and high angular-momentum gas in galactic halos can produce extended halo structures whose dynamical influence becomes approximately spherical on large scales [36–38]. The spherical reconstruction used here should therefore be regarded as a practical approximation capturing this large-scale behaviour

For each galaxy χ was the only free parameter, while the baryonic contribution was fixed directly from the SPARC photometric data. The value of χ was determined by iteratively solving eq. (52) and imposing a normalization condition in the outer disk $\langle V_\chi\rangle_{\rm outer} = \langle V_{\rm obs}\rangle_{\rm outer}$, where the averages are taken over the outer $\sim 30\%$ of radial data points. This procedure fixes the overall amplitude of the model rotation curve while leaving its radial shape determined by the solution of eq. (52). To quantify the quality of the fit, the weighted RMS residual $\mathrm{wRMS} = \sqrt{\frac{\sum_i w_i (V_{\rm obs}-V_\chi)^2}{\sum_i w_i}}$ is computed over the entire radial range of the rotation curve using observational uncertainties as weights. Because the outer normalization condition enforces agreement at large radii, additional diagnostics are reported separately for the inner and intermediate regions of the rotation curve. A summary table containing, for each galaxy, the fitted χ, the weighted RMS residual over the full radial range (wRMS), the residuals for the inner and intermediate radial regions, the quality parameter $Q \equiv \frac{\mathrm{wRMS}}{\langle V_{\rm obs}\rangle_{\rm outer}}$, a quality flag (A-C) derived from Q, and the number of data points used in the fit (N) is provided in A. Quality flags correspond to $Q < 0.10$ (A), $0.10 \le Q < 0.20$ (B), and $Q \ge 0.20$ (C)

© 2026 by the author(s). Distributed under a Creative Commons CC BY license.

Preprints.org (www.preprints.org) | NOT PEER-REVIEWED | Posted: 9 March 2026 doi:10.20944/preprints202510.1554.v7

The full fitting pipeline, including reading the SPARC rotation-curve data, interpolating the baryonic component $V_{\rm bar}(r)$, reconstructing the spherical proxy density, numerically solving eq. (52), and exporting the rotation-curve plots and statistical tables, was fully automated in the accompanying Mathematica script, which is included in the supplementary material

To provide a benchmark for the quality of fit, a comparison was made between the Alena Tensor model in the constant parameter approximation χ and two commonly used, low-parameter descriptions of rotation curves:

- MOND with the classical acceleration scale value a_0
- one-parameter approximation of the core-type halo profile (here designated Burkert-1p), in which the halo component amplitude is fixed by normalization in the outer disk (analogous to the normalization procedure in AT).

All wRMS values were calculated on the same SPARC points and with the same weights (inverse of the variance of the velocity errors). The summary table in B shows that out of 104 analysed galaxies, the AT model yields $\mathrm{wRMS}_{\rm AT} \le \mathrm{wRMS}_{\rm MOND}$ in 85 cases and $\mathrm{wRMS}_{\rm AT} \le \mathrm{wRMS}_{\rm Burkert}$ in 82 cases, corresponding to approximately 82% and 79% of the sample, respectively. The Burkert-1p column represents a simplified one-parameter cored-halo proxy used purely as a benchmark reference, rather than a full two-parameter Burkert halo fit. The AT model normalization follows the same outer-disk velocity matching procedure used for the one-parameter halo proxy

Additionally, it was examined whether the fitted χ values correlate with galaxy properties

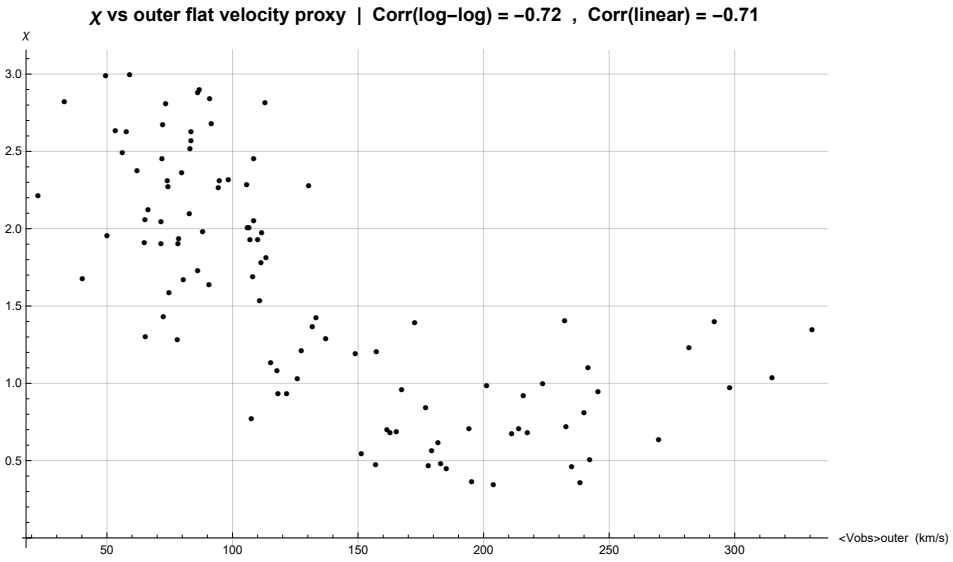

Figure 2. The dependence of the fitted parameter χ on $\langle V_{\rm obs}\rangle_{\rm outer}$

As a simple, uniformly accessible measure of the dynamical state, it was used $\langle V_{\rm obs}\rangle_{\rm outer}$, i.e., the mean velocity observed in the outer part of the rotation curve (the last $\sim 30\%$ radial points). Fig. 2 shows the dependence of χ on $\langle V_{\rm obs}\rangle_{\rm outer}$, along with the given correlation coefficients (on a linear and log-log scale). The observed high correlation suggests that χ is not merely a free per-galaxy tuning parameter, but may encode a systematic scaling with galaxy dynamical properties

It is also worth emphasizing that the discussed framework leads to concrete and testable observational predictions for gravitational lensing. In this approach, the halo effect is not associated with an additional mass component, but emerges from rotational energy, energy fluxes, and anisotropic stresses contained in the matter energy-momentum tensor. In the general formulation, lensing is governed by the Ricci focusing term obtained from the contraction with a null vector $k^\mu = \varpi\left(\frac{U^\mu}{c} + n^\mu\right)$ which yields, using Einstein equations

$$R_{\mu\nu}k^\mu k^\nu = \kappa\, T_{\mu\nu}k^\mu k^\nu = \kappa\,\varpi^2\left[\rho c^2 + 3\mathcal{E}_{\rm rot} + \frac{2}{c}(q^\mu n_\mu) - \tau^{\mu\nu}n_\mu n_\nu\right] \tag{55}$$

© 2026 by the author(s). Distributed under a Creative Commons CC BY license.

Preprints.org (www.preprints.org) | NOT PEER-REVIEWED | Posted: 9 March 2026 doi:10.20944/preprints202510.1554.v7

The relation between the Ricci focusing term and gravitational lensing follows from the Sachs optical equations for a bundle of null geodesics, as derived in eqs. (2.6-2.12) of [39]. In particular, the expansion θ of the light bundle satisfies

$$\frac{d\theta}{d\lambda} = -\frac{1}{2}\theta^2 - \sigma^2 - R_{\mu\nu}k^\mu k^\nu \tag{56}$$

where λ is the affine parameter and σ is the shear of the null congruence. In the weak-lensing regime the quadratic terms can be neglected, so that the focusing is directly controlled by the Ricci contraction $R_{\mu\nu}k^\mu k^\nu$. Similar sensitivity of gravitational lensing to anisotropic stress is known to appear in relativistic weak-lensing formalisms [40]. This expression shows explicitly that, in addition to the effective energy density $\rho c^2 + 3\mathcal{E}_{\rm rot}$, lensing is sensitive to energy fluxes q^μ and anisotropic stresses $\tau^{\mu\nu}$, which encode angular momentum transport and are responsible for the halo-like behavior in the Alena Tensor model. A simpler and more practical observational test can be constructed using the idealized fluid approximation $T^{\mu\nu}_{\rm ideal}$, supplemented by an effective anisotropy parameter χ, defined through directional pressures. In the thin-lens approximation the observable lensing convergence $\kappa_{\rm lens}$ is determined by the projection of this quantity along the line of sight [39]

$$\kappa_{\rm lens}(R) = \frac{1}{\Sigma_{\rm crit}} \int dz \, \frac{T_{\mu\nu}k^\mu k^\nu}{c^2\varpi^2} \tag{57}$$

This expression is formally equivalent to the standard weak-lensing relation $\kappa_{\rm lens} = \Sigma/\Sigma_{\rm crit}$, which allows one to define an effective surface density $\Sigma_{\rm eff}$ through the projection of the stress-energy contribution along the line of sight. Here ϖ denotes the normalization of the null vector $k^\mu = \varpi(U^\mu/c + n^\mu)$, so that $T_{\mu\nu}k^\mu k^\nu/\varpi^2$ corresponds to the physically relevant projection T_{kk}. In this case, the Ricci focusing reduces to the form below, which directly translates into an effective surface density for lensing

$$\frac{T_{kk}}{\varpi^2} = \rho c^2 + 2p + p_r n_r^2 + p_\theta n_\theta^2 + p_\phi n_\phi^2 \quad ; \quad \Sigma_{\rm eff}(R) = \int dz \left[\rho + W(i)\frac{p}{c^2}\right] \tag{58}$$

where the weight $W(i)$ depends on the inclination i of the system with respect to the line of sight. For a disk galaxy, this leads to two limiting cases:

$$\Sigma^{\rm face}_{\rm eff} = \int dz \left[\rho + \left(2 + \frac{\chi}{2}\right)\frac{p}{c^2}\right] \quad ; \quad \Sigma^{\rm edge}_{\rm eff} = \int dz \left[\rho + \left(\frac{5}{2} + \frac{\chi}{4}\right)\frac{p}{c^2}\right] \tag{59}$$

Consequently, one generically predicts

$$\Sigma^{\rm face}_{\rm eff} - \Sigma^{\rm edge}_{\rm eff} = \frac{\chi - 2}{4}\Sigma_p \quad ; \quad \Sigma_p \equiv \int dz \, \frac{p}{c^2} \tag{60}$$

and thus a systematic inclination-dependent lensing signal whose sign and magnitude are directly controlled by the anisotropy parameter χ, for systems with identical baryonic mass distributions and rotation curves. This inclination-dependent lensing signal provides a simple and robust observational test of the Alena Tensor halo mechanism, which is not expected in standard isotropic dark matter halo models, but is indicated by the conclusions from observations e.g. in [41–43]

3.2. Quantum vortices and elementary particles

In chapter 2.2.1 the possibility of quantum analysis of the Alena Tensor was demonstrated, so it is worth making such a preliminary analysis. The simplified effective Lagrangian shown below can be considered as a low-energy approximation of the quantum Lagrangian $\mathcal{L}_Q$ from (31), obtained after integrating the degrees of freedom associated with the rotational sector of the Alena Tensor, serving as phenomenological low-energy model capturing the dominant rotational response. In this sense,

© 2026 by the author(s). Distributed under a Creative Commons CC BY license.

Preprints.org (www.preprints.org) | NOT PEER-REVIEWED | Posted: 9 March 2026 doi:10.20944/preprints202510.1554.v7

the function χ_ω is no longer an independent geometric field, but appears as a local four-dimensional operator, while retaining exactly the same energy interpretation and vacuum screening mechanism.

$$\begin{aligned}\mathcal{L}_{\text{eff}} &= \underbrace{\frac{\hbar c}{2}(\partial_\mu\rho)(\partial^\mu\rho) + \frac{\hbar c}{2}\rho^2(\partial_\mu\phi)(\partial^\mu\phi)}_{\mathcal{L}_{\text{scalar(vortex)}}} + \underbrace{\bar\psi\Big(i\hbar c\,\gamma^\mu D_\mu - mc^2\Big)\psi}_{\mathcal{L}_\psi} \\ &+ \underbrace{\frac{e^{-\vartheta(\rho)}}{2c^2\kappa}\omega_{\mu\nu}\omega^{\mu\nu} - g\hbar\,\bar\psi\Sigma_{\mu\nu}\psi\,\omega^{\mu\nu}}_{\mathcal{L}_{\text{spin-vortex}}} \end{aligned} \tag{61}$$

where

- $\phi(x)$ - vortex phase field (action phase). Its gradient $\partial_\mu\phi$ represents the generalized four-momentum flow associated with the vortex structure.
- $\rho(x)$ - amplitude of the complex condensate $\varphi = \hbar c\rho\, e^{i\phi}$. It determines the vortex core profile and sets the symmetry-breaking scale.
- $\omega_{\mu\nu}$ - vorticity tensor of the underlying medium. In this Lagrangian it is treated as an independent antisymmetric field capturing local rotational structure analogous to the Hubbard-Stratonovich transformation [44].
- $\Sigma_{\mu\nu}$ - spin generator in the fermionic representation $\Sigma_{\mu\nu} = \frac{i}{4}[\gamma_\mu, \gamma_\nu]$.
- $e^{\vartheta(\rho)}$ - plays the role of a dimensionless state-dependent stiffness function, encoding the effective elastic response of the vortex condensate, where it is assumed for calculation simplicity $p_\Lambda\alpha = e^{-\vartheta(\rho)}/(c^2\kappa)$
- g - dimensionless spin-vorticity coupling constant, determining the strength of the interaction between fermionic spin and the vortex background.

The Madelung decomposition $\varphi = \hbar c\,\rho\, e^{i\phi}$ introduces an effective phase field whose gradient gives the conserved current $\hbar c\,\rho^2\,\partial^\mu\phi$

It may be also assumed that the electroweak symmetry is broken by a chiral fermion condensate $\langle\bar\psi_R\psi_L\rangle \neq 0$ which implies $SU(2)_L \times U(1)_Y \to U(1)_{\text{em}}$. The associated three Goldstone modes are thus absorbed as the longitudinal polarizations of $W^\pm$ and Z bosons, yielding their masses in the standard, technicolor way. The Higgs boson is also identified with the lightest scalar resonance in the technicolor sector associated with the chiral condensate $\langle\bar\psi_R\psi_L\rangle \neq 0$, as in standard technicolor constructions [45,46]. However, the mechanism of fermion generation may result from the adopted Lagrangian

In the next steps it will be shown that by treating the Lagrangian (61) as an effective field model and choosing an appropriate stiffness function $\vartheta(\rho)$, the effective description admits structures analogous to Yukawa-type mass generation and Higgs-like potentials

The vorticity tensor enters the Lagrangian (61) only through the elastic term and the spin-vorticity interaction. Its algebraic equation of motion yields

$$\frac{\partial\mathcal{L}_{\text{eff}}}{\partial\omega^{\mu\nu}} = 0 \quad \to \quad \omega_{\mu\nu} = c^2\kappa\, e^{\vartheta(\rho)}\, g\hbar\,\bar\psi\Sigma_{\mu\nu}\psi \tag{62}$$

so that eliminating $\omega_{\mu\nu}$ produces the effective fermion term

$$\mathcal{E}_{rot} = \frac{g^2\hbar^2c^2\kappa\, e^{\vartheta(\rho)}}{2}(\bar\psi\Sigma^{\mu\nu}\psi)(\bar\psi\Sigma_{\mu\nu}\psi) \tag{63}$$

Evaluated at the homogeneous equilibrium, this yields a dynamically generated fermion mass

$$m_{\text{eff}} = \frac{g^2\hbar^2\kappa\, e^{\vartheta(\rho)}}{2}\langle\Sigma\rangle \quad ; \quad \langle\Sigma\rangle \equiv \frac{\langle(\bar\psi\Sigma^{\mu\nu}\psi)(\bar\psi\Sigma_{\mu\nu}\psi)\rangle}{\langle\bar\psi\psi\rangle} \tag{64}$$

© 2026 by the author(s). Distributed under a Creative Commons CC BY license.

Preprints.org (www.preprints.org) | NOT PEER-REVIEWED | Posted: 9 March 2026 doi:10.20944/preprints202510.1554.v7

Up to Fierz rearrangements [47], the induced four-fermion operator contains a scalar channel allowing for fermion mass generation, analogously to NJL-type dynamics [48]. In this picture, the mass generation results from the equilibrium between the scalar amplitude ρ and the spin-vorticity background, rather than from a fundamental Yukawa coupling where the condensate $\langle\Sigma\rangle$ plays the role of an order parameter. For a stationary vortex configuration $\varphi = \hbar c\rho\, e^{i\phi}$, the scalar sector of (61) thus leads to the standard energy functional

$$E[\rho,\phi] = \frac{\hbar c}{2}\int d^3x\,\left[(\nabla\rho)^2 + \rho^2(\nabla\phi)^2\right] \tag{65}$$

Euler-Lagrange equations derived from (61) are

$$\hbar c\,\partial_\mu\partial^\mu\rho - \left[\hbar c\,\rho\,(\partial_\mu\phi)(\partial^\mu\phi) - \frac{\vartheta'(\rho)e^{-\vartheta(\rho)}}{2c^2\kappa}\,\omega_{\alpha\beta}\omega^{\alpha\beta}\right] = 0\,;\;\partial_\mu\Big(\rho^2\,\partial^\mu\phi\Big) = 0 \tag{66}$$

and show that the amplitude adjusts to the local phase gradient. In the presented model, ρ has the dimension of the inverse of the length while Standard Model vev $v_{\rm SM}$ is expressed as energy. Considering the equations in the limit $\rho = v$ one may thus assume that $\hbar c v \equiv v_{\rm SM}$ which fixes the normalization of the scalar amplitude and should be understood as a matching condition between the effective vortex sector and the electroweak vacuum scale. Since the effective Yukawa parameter can be extracted directly from (64) therefore in order to reproduce the Standard Model it should satisfy $m_{\rm eff}c^2 = \frac{y_{\rm f}}{\sqrt{2}}\,\hbar c\,v$, thus

$$\frac{y_{\rm f}\hbar c}{\sqrt{2}} \equiv \frac{\partial m_{\rm eff}(\rho)c^2}{\partial\rho}\bigg|_{\rho=v} = m_{\rm eff}c^2\,\vartheta'(v) \;\rightarrow\; \frac{\hbar c\,y_{\rm f}}{\sqrt{2}\,m_{\rm eff}c^2} = \frac{1}{v} \;\rightarrow\; \vartheta'(v) \equiv \frac{1}{v} \tag{67}$$

Assuming the stationary energy-minimizing configuration (static state)

$$\rho(x) = v = \text{const} \quad ; \quad \partial_{\rm i}æ = 0 \quad ; \quad Œ(x) = {}^{-}{\rm ct} \quad ; \quad \partial_{\rm i}Œ = 0 \tag{68}$$

the Euler-Lagrange equation for $\rho = v$ reduces therefore to

$$\mathcal{E}_{rot}(v) = m_{\rm eff}c^2\,\langle\bar\psi\psi\rangle = \frac{e^{-\vartheta(v)}}{2c^2\kappa}\,\omega_{\alpha\beta}\omega^{\alpha\beta} = \hbar c\,\frac{v\,\mu^2}{\vartheta'(v)} = \hbar c\,v^2\mu^2 \tag{69}$$

Under suitable assumptions on the stiffness function $\vartheta(\rho)$ and on the spin-vorticity condensate encoded in $\omega_{\alpha\beta}\omega^{\alpha\beta}$, this relation plays the role of a gap equation, equivalent to the condition $\partial V_{\rm eff}(\rho)/\partial\rho|_{\rho=v} = 0$ for an effective Higgs-like potential. The competition between $\mathcal{E}_{rot}$ and $\hbar c\,v^2\mu^2$ might therefore reproduce the characteristic symmetry-breaking structure of the Higgs potential. Using the equilibrium equation and the condition $\vartheta'(v) = \frac{1}{v}$, the second derivative of the effective potential can be calculated as

$$\frac{\partial^2 V_{\rm eff}(\rho)}{\partial\rho^2}\bigg|_{\rho=v} = m_{\rm eff}c^2\,\langle\bar\psi\psi\rangle\left[\vartheta''(v) + \big(\vartheta'(v)\big)^2 - \frac{\vartheta'(v)}{v}\right] = m_{\rm eff}\,c^2\langle\bar\psi\psi\rangle\,\vartheta''(v) \tag{70}$$

Equivalently, assuming that the effective potential $V_{\rm eff}(\rho)$ is indeed of Higgs type, it may also be assumed that

$$\frac{\partial^2 V_{\rm eff}(\rho)}{\partial\rho^2}\bigg|_{\rho=v} \equiv 2\hbar c v^2 \tag{71}$$

© 2026 by the author(s). Distributed under a Creative Commons CC BY license.

Preprints.org (www.preprints.org) | NOT PEER-REVIEWED | Posted: 9 March 2026 doi:10.20944/preprints202510.1554.v7

Therefore (70) = (71) may be further simplified, imposing a specific form on the function $\vartheta(\rho)$ as below, for the preservation of the Yukawa condition and the Higgs-like potential

$$\begin{aligned} \vartheta(\rho) &\equiv \ln\frac{\rho}{v} + \frac{\coth^2\left(\frac{\theta_f}{2}\right)}{2}\left(\frac{\rho}{v}-1\right)^2 \quad \rightarrow \\ \mathcal{E}_{rot}(v) &= m_{\text{eff}}c^2\,\langle\bar{\psi}\psi\rangle = 2\hbar c v^2\,\frac{v^2}{\coth^2\left(\frac{\theta_f}{2}\right)-1} = 2\hbar c v^4\sinh^2\left(\frac{\theta_f}{2}\right) \end{aligned} \tag{72}$$

The chosen form of $\vartheta(\rho)$ is the minimal analytic function satisfying simultaneously the Yukawa condition, vacuum normalization, and positivity of the Higgs curvature. It yields

$$\frac{y_f}{\sqrt{2}}\cdot\langle\bar{\psi}\psi\rangle = 2\sinh^2\left(\frac{\theta_f}{2}\right)\cdot v^3 \tag{73}$$

Therefore, following standard dimensional estimates for strongly coupled fermion condensates one may make the natural assumption $\langle\bar{\psi}\psi\rangle = v^3$, and separate condensate from Yukawa parameter as follows

$$\frac{y_f}{\sqrt{2}} = \frac{\mu^2}{v^2} = 2\sinh^2\left(\frac{\theta_f}{2}\right) = \cosh(\theta_f) - 1 \tag{74}$$

replacing the Yukawa parameter y_f with square of the ratio of the topological energy of the vortex to the electroweak vacuum scale. In this picture $\cosh(\theta_f) - 1$ determines the total excess energy needed to maintain the phase current where $A = 2\sinh\left(\frac{\theta_f}{2}\right)$ can be interpreted as the amplitude of the underlying spinor wave ψ, representing a propagating, localized excess of energy above the vacuum background $\rho = v$ and carrying spin $1/2$

In this way the above approach suggests an interpretation of elementary fermions as stable quantum vortices, reproducing structural features analogous to the Yukawa and Higgs mechanisms, where all stability requirements follow directly from the field equations and the structure of the effective potential. In this approach, the technicolor sector is responsible for the vacuum dynamics leading to the spontaneous breaking of the electroweak symmetry and the establishment of the v_{SM} scale, while the fermions are treated as effective excitations of this vacuum of a topological nature, described by an independent vortex sector

This interpretation is fully consistent with the general paradigm of topological solitons, where localized and finite-energy excitations of a continuous field behave as particle-like objects, as in the Skyrme model [49,50], the Faddeev-Niemi hopfion model [51,52], and the superfluid-vacuum approach of Volovik [53]. In the presented case, the spin-vorticity coupling and the rotational energy functional play the role of stabilizing terms, ensuring that the vortex configuration propagates as a massive fermionic quasiparticle, closely analogous to knotted vortical solitons in classical and quantum field theories [54]

One may also notice that this type of effective Lagrangian (61) naturally supports four distinct conserved charges, arising from its symmetries and from the structure of the vorticity sector (with accuracy to constants)

- *Phase (Noether) charge* $Q_\phi = \int d^3x\, j^0 \quad ; \quad j^\mu \equiv \rho^2\,\partial^\mu\phi$ originating from the global shift symmetry. It corresponds to the conserved circulation associated with the phase field.
- *Topological vortex number* $N_v = \frac{1}{2\pi}\oint_{\mathcal{C}}\nabla\phi\cdot d\vec{\ell} \in \mathbb{Z}$ defined for static configurations with nontrivial winding of the phase ϕ around the vortex core. This integer counts the number of 2π windings.
- *Spin-vorticity flux charge* $Q_{\text{sv}} = \int d^3x\,\partial_\mu(g\hbar\,\omega^{\mu 0})$ where the vorticity tensor $\omega_{\mu\nu}$ satisfies the algebraic field equation $\omega_{\mu\nu} = c^2\kappa\, e^{\vartheta(\rho)} g\hbar\,\bar{\psi}\Sigma_{\mu\nu}\psi$. This charge reflects the conserved flow associated with the spin-vorticity coupling term $g\hbar\,\bar{\psi}\Sigma_{\mu\nu}\psi\,\omega^{\mu\nu}$.
- *Hopf (linking) charge* $Q_H = \frac{1}{32\pi^2}\int d^3x\,\epsilon^{ijk}\,\mathcal{A}_i\,\mathcal{F}_{jk}$ defined when the dual vorticity vector $\omega_i \equiv \frac{1}{2}\epsilon_{ijk}\omega_{jk}$ is normalized to a unit field $\vec{n}(x) = \vec{\omega}/|\vec{\omega}|$, with $\mathcal{F}_{ij} = \partial_i\mathcal{A}_j - \partial_j\mathcal{A}_i$ denoting the pullback

© 2026 by the author(s). Distributed under a Creative Commons CC BY license.

Preprints.org (www.preprints.org) | NOT PEER-REVIEWED | Posted: 9 March 2026 doi:10.20944/preprints202510.1554.v7

of the area form on S^2. This integer-valued invariant characterizes the knotting and linking of vorticity lines.

It is therefore possible to expand the model based on the conserved charges and deeper analysis of the model in the context of reproducing known structural features of elementary particles, including the possibility of identifying particle families with different topological sectors.

It may be also noticed that assuming non-zero particle's mass m, variation of (61) with respect to $\bar{\psi}$ gives the modified Dirac equation

$$\left(i\hbar c\,\gamma^{\mu}D_{\mu} - mc^2 - g\hbar\,\Sigma^{\mu\nu}\omega_{\mu\nu}\right)\psi = 0 \tag{75}$$

where the last term is a local spin-vorticity coupling formally analogous to the Mashhoon effect [55,56]. For the normalization of $\omega_{\mu\nu}$ assumed in (13) this correspondence fixes $g = \frac{1}{2}$. This allows the obtained model to be applied to atomic systems and other classical settings

One may consider the regime in which the effective vorticity field $\omega_{\mu\nu}$ is dominated by a stationary rotational background with angular velocity $\vec{\Omega}$. Using the standard identification of spatial components $\omega^i = \frac{1}{2}\epsilon^{ijk}\omega_{jk}$, the nonrelativistic Foldy-Wouthuysen expansion as in [57] therefore yields an additional spin-rotation term in the effective Hamiltonian $\Delta H_{\mathrm{sv}} = -\frac{1}{2}\,\hbar\,\vec{\sigma}\cdot\vec{\Omega}$ corresponding to a rotation-induced spin splitting $\Delta E = \hbar|\Omega|$. This effect is directly testable in precision spin-precession experiments, atomic and neutron interferometry, and high-resolution spectroscopy in controlled rotating platforms

The vacuum normalization $e^{\vartheta(v)} = 1$ ensures that the coupling is fixed in vacuum and coincides with the standard spin-rotation interaction, while any deviation must arise from medium-dependent effects encoded in $\rho \neq v$. Consequently, the quantum sector of the Alena Tensor framework leads to two distinct and falsifiable implications:

- a fixed, parameter-free spin-rotation coupling in vacuum, reproducing the Mashhoon-type precession without additional degrees of freedom,
- a possible environment-dependent modification of spin-dependent interactions,

constrained by precision limits on anomalous spin couplings in vortical or rotating media. Any observed departure from the vacuum prediction thus directly bounds the response function $e^{\vartheta(\rho)}$, providing an experimental handle on the rotational sector of the theory. The available literature indicates that the described effect is expected [58], already observed to some extent [59] and should be measurable using standard research procedures [60,61]

4. Discussion and Conclusions

It is worth discussing the conclusions of this article by dividing them into issues concerning GR/Cosmology and quantum issues

4.1. Discussion and Conclusions Regarding GR and Cosmology

As seen in the above article, supplementing the Alena Tensor with the energy associated with the rotation of bodies naturally leads to the creation of halo effects, known from dark matter studies. Preliminary analysis allows for a fairly good match of this effect to observational results, although this obviously requires further development and verification for a larger number of cosmological objects. Importantly, the proposed approach does not require modification of the GR equations, but rather fits naturally into the applied GR equations and continuum mechanics. The model discussed also describes the properties related to gravitational lensing, however, a dedicated analysis of light deflection, including the role of anisotropic stresses, would be required to quantitatively assess the consistency of the model with lensing observations [39,62]. In standard NFW dark matter halos or in MOND-like modified gravity models, the lensing signal at fixed baryonic mass and rotation curve is expected to be largely insensitive to disk inclination, apart from trivial geometric projection effects. As shown in 3.1, the predicted inequality $\Sigma_{\mathrm{eff}}^{\mathrm{face}} - \Sigma_{\mathrm{eff}}^{\mathrm{edge}}$ makes therefore a distinctive and falsifiable

© 2026 by the author(s). Distributed under a Creative Commons CC BY license.

Preprints.org (www.preprints.org) | NOT PEER-REVIEWED | Posted: 9 March 2026 doi:10.20944/preprints202510.1554.v7

signature of the Alena Tensor framework. This inclination-dependent lensing imprint has not yet been explored in dedicated observational studies and given the availability of large galaxy-galaxy lensing samples and resolved kinematic data, the proposed signal appears readily testable

The proposed solution fits quite well with the research direction represented by [63–65] and also [66] (including baryotropy), who investigated anisotropic fluid in cosmology and its potential connections with the dark sector. Related directions have also been explored in recent studies that model the dark sector as an effective relativistic fluid or emergent gravitational component, where halo phenomenology and galaxy rotation curves arise from modified stress-energy structures rather than from additional particle degrees of freedom [67–69]. However, it complements these studies with the natural halo effect resulting directly from the GR equations for the Alena Tensor. The proposed model also expands and, in a sense, substantiates the hypothesis posed by C. Rourke [70], complementing the research [71–74] with a justification for linking rotation with the halo effect. The idea that geometric contributions can mimic dark matter is not new [75,76], but Alena Tensor gives it some additional structure, making it a direct consequence of a coherent mathematical model

Importantly, the Alena Tensor also provides a natural interpretation of dark energy. The value of p_Λ is an invariant of the field tensor and becomes constant (or, at least, metric-independent invariant) in curvilinear description. In a sense, a nonzero value of Λ can therefore be interpreted as a scale of deviation from pure wave solutions, without matter (for example, for the electromagnetic field, $p_\Lambda = 0$ would mean that the electric and magnetic fields are equal, so the solutions must be pure electromagnetic waves). Since the value of p_Λ measured in flat spacetime is $p_\Lambda = p_o\left(\mathbb{k}_{\mu\nu}\eta^{\mu\nu}\right)^2$, it is a measure of the "flatness" of spacetime, or more precisely, a measure of how much the metric tensor for the curvilinear description deviates from the Minkowski tensor. This interpretation seems particularly interesting in the context of the works [77,78], because it strengthens and details the conclusions described therein, providing a geometric, anisotropic source that can be interpreted as a specific backreaction mechanism leading to acceleration. Whether this identification can fully reproduce the phenomenology of dark energy at the level of background expansion and cosmological perturbations remains an open question and should be addressed in future work

It seems that the next best step would be to conduct consistent tests of gravitational lensing (in galaxies and clusters), satellite dynamics, and perturbation cosmology (structure growth, ISW, CMB), which would allow to clearly confirm or falsify the assumptions presented in the article. This approach could be also applied to many other continuous systems (e.g., stars or black holes) which would allow for the analysis of its further, yet unseen properties.

4.2. Discussion and Conclusions Regarding Quantum Issues

In quantum theory, the same structure of the energy-momentum tensor gives rise to topological vortices whose stability determines states with interpretable mass. The analysis presented in this work indicate the possibility of effective-field reinterpretation of the Higgs mechanism in terms of vortex dynamics, in which fermion masses arise from a self-consistent spin-vorticity condensation rather than from fundamental Yukawa couplings. The elimination of the antisymmetric vorticity field leads to an effective four-fermion interaction and a gap equation for the condensate modulus, allowing for particle-like, topologically stabilized vortex excitations to emerge within the obtained Belinfante energy-momentum tensor structure

The inclusion of rotational energy contributions in the energy-momentum tensor naturally induces a local spin-vorticity coupling, encoded in the modified Dirac equation (75). In the nonrelativistic limit this coupling reduces to a Mashhoon-type interaction, consistent with earlier analyses of inertial and rotational effects in relativistic quantum mechanics [79–81]. Such couplings are known to play a role in systems with significant vorticity, including relativistic fluids and rotating quantum media, where spin polarization effects have been discussed in hydrodynamic and condensed-matter contexts [82,83]. In this sense, the obtained vorticity field admits a direct physical interpretation as an effective rotational background, potentially relevant for vortical quantum systems such as the quark-gluon plasma [84]

© 2026 by the author(s). Distributed under a Creative Commons CC BY license.

Preprints.org (www.preprints.org) | NOT PEER-REVIEWED | Posted: 9 March 2026 doi:10.20944/preprints202510.1554.v7

The effective theory exhibits four conserved quantities: the phase charge Q_ϕ, the vortex number N_v, the spin-vorticity charge $Q_{\rm sv}$, and the Hopf charge Q_H. These invariants classify vortex configurations according to their topology and are closely analogous to conserved charges appearing in well-established soliton models, including Skyrme-type constructions [85], Faddeev-Niemi hopfions [86], and related knot-like soliton solutions [87,88]. Within the present approach, fermionic excitations may be associated with stable, spin-carrying vortex configurations, while different topological sectors could encode additional structural distinctions among particle-like solutions

Eliminating the vorticity field yields an effective description reminiscent of dynamical mass generation mechanisms known from Nambu-Jona-Lasinio models [89], composite Higgs scenarios [90,91], and superfluid-vacuum analogies [53]. In this picture, the Higgs boson appears as a radial excitation of the condensate, with its mass determined by the curvature of the effective potential. While the present analysis remains at the level of an effective model, it suggests a unified perspective on fermion and Higgs mass generation tied to vortex stability and the structure of the condensate

The results obtained here motivate several directions for further study, including the construction of fully nonlinear three-dimensional vortex solutions with prescribed topological charges, the analysis of their stability and energetics, and the investigation of possible phenomenological implications of spin-vorticity couplings. Potential applications range from atomic and condensed-matter systems to relativistic heavy-ion collisions [82,92] and astrophysical settings such as neutron stars [93,94]. A more detailed exploration of transport properties and spin polarization effects in vortical media [95,96] may further clarify the physical relevance and limitations of the proposed framework

Equally interesting direction of further analysis could be e.g. the use of the possibilities of quantum description of the dark sector in the Alena Tensor model, for further development of works such as [97]. It also seems that describing matter (e.g. a neutron star, as in [98,99]) using the mechanism proposed here for GR, would be the simplest way to confirm or falsify the Alena Tensor, due to the high symmetry of such a solution. It can also be noted that the Madelung phase ϕ obtained in this paper may be e.g. interpreted as the phase of microscopic proper-time oscillations of spacetime, analogous to the scalar field ζ considered in the [100] introduced in spacetime excitation model. In this picture, the localized vortex solutions would correspond to stable, topologically protected configurations of the underlying spacetime phase. However, all these analyses deserve separate articles

In conclusion, it remains an open question whether the Alena Tensor is a correct way to describe physical systems, but this paper shows that, beyond the compliances with available knowledge achieved so far, it naturally leads to the existence of halo effects, interpretation of dark energy and modeling quantum vortices. Taken together, these results indicate that the extended Alena Tensor offers a unified geometric and topological framework that connects elementary particles, relativistic fluids and large-scale astrophysical structures. This opens a way for theoretical and phenomenological studies, extending far beyond the cosmological applications emphasized in the present work

The author hopes that the results obtained in this paper will facilitate further use and development of the discussed approach and, potentially, many similar concepts. It also seems that further analysis of Alena Tensor may provide useful descriptions of the transformation between curved and flat spacetime and bring new insights that will contribute to a better understanding of issues related to the broadly understood unification of physical theories.

5. Statements

All data that support the findings of this study are included within the article (and any supplementary files)

During the preparation of this work the author did not use generative AI or AI-assisted technologies, except for continuous learning

Author did not receive support from any organization for the submitted work

Author have no relevant financial or non-financial interests to disclose

© 2026 by the author(s). Distributed under a Creative Commons CC BY license.

Preprints.org (www.preprints.org) | NOT PEER-REVIEWED | Posted: 9 March 2026 doi:10.20944/preprints202510.1554.v7

Appendix A Numerical results of fitting the constant χ

Table A1. Goodness-of-fit statistics for the constant-χ model. wRMS(all) is computed over the full radial range. wRMS(inner) and wRMS(mid) are computed over the inner 30% and middle 40% of radial points (sorted by radius). The fit normalisation enforces agreement in the outer region.

Galaxy	χ	wRMS(all) [km/s]	wRMS(inner) [km/s]	wRMS(mid) [km/s]	Q = wRMS/$\langle V_{\rm obs}\rangle_{\rm outer}$	Flag	N
D631-7	2.631	7.2	8.5	7.3	0.126	B	16.
DDO161	2.125	3.1	6.8	4.1	0.047	A	31.
DDO168	2.640	4.1	6.0	3.5	0.077	A	10.
DDO170	2.997	5.6	8.7	6.5	0.094	A	8.
ESO079-G014	1.395	7.1	21.9	11.6	0.041	A	15.
ESO116-G012	1.931	5.5	9.6	6.1	0.050	A	15.
ESO563-G021	1.038	32.3	42.6	15.2	0.102	B	30.
F568-3	2.458	6.7	4.3	11.6	0.061	A	18.
F568-V1	2.814	19.0	19.4	20.7	0.168	B	15.
F571-8	1.369	45.8	63.4	52.6	0.347	C	13.
F574-1	2.319	5.7	5.2	7.8	0.058	A	14.
F579-V1	1.817	18.6	28.1	15.4	0.164	B	14.
F583-4	2.062	2.6	4.3	1.9	0.040	A	12.
IC4202	0.510	41.5	52.5	20.5	0.172	B	32.
KK98-251	2.822	1.1	0.6	0.6	0.033	A	15.
NGC0024	1.933	7.2	9.7	8.2	0.068	A	29.
NGC0055	1.733	3.9	6.7	1.6	0.045	A	21.
NGC0100	1.983	8.8	11.3	8.6	0.100	B	21.
NGC0247	2.287	9.2	10.2	0.8	0.087	A	26.
NGC0289	0.960	31.8	59.7	29.5	0.190	B	28.
NGC0300	2.267	2.3	2.5	2.8	0.025	A	25.
NGC1003	1.782	13.0	18.3	14.9	0.117	B	36.
NGC1090	0.682	16.3	36.2	21.6	0.100	B	24.
NGC1705	1.906	2.7	5.6	0.5	0.038	A	14.
NGC2366	1.959	3.8	5.3	3.3	0.077	A	26.
NGC2403	1.430	17.8	21.3	20.6	0.133	B	73.
NGC2683	0.475	24.8	33.1	15.7	0.158	B	11.
NGC2841	1.232	17.8	11.9	25.4	0.063	A	50.
NGC2903	0.484	51.1	105.4	51.2	0.279	C	34.
NGC2915	2.100	8.2	19.9	2.4	0.099	A	30.
NGC2998	0.676	14.1	26.5	22.8	0.067	A	13.
NGC3198	1.192	22.1	24.7	26.9	0.149	B	43.
NGC3726	0.700	36.3	44.9	37.0	0.224	C	12.
NGC3741	2.991	2.6	3.0	3.2	0.053	A	21.
NGC3769	1.085	26.2	44.3	19.3	0.222	C	12.
NGC3893	0.570	34.4	50.5	23.2	0.192	B	10.
NGC3917	1.292	5.1	9.0	1.0	0.037	A	17.
NGC3972	1.211	5.1	6.0	3.4	0.040	A	10.
NGC3992	0.949	9.9	20.5	5.4	0.040	A	9.
NGC4010	1.031	12.5	18.2	15.5	0.099	A	12.
NGC4013	0.843	33.0	44.3	30.9	0.187	B	36.
NGC4100	0.687	12.5	19.2	10.8	0.075	A	24.
NGC4157	0.447	47.8	68.8	47.7	0.258	C	17.
NGC4183	1.540	4.6	7.4	3.8	0.042	A	23.
NGC4214	1.675	8.8	13.9	6.2	0.110	B	14.
NGC4559	0.938	16.8	29.4	15.1	0.139	B	32.
NGC5033	0.706	29.1	95.8	27.2	0.150	B	22.

© 2026 by the author(s). Distributed under a Creative Commons CC BY license.

Preprints.org (www.preprints.org) | NOT PEER-REVIEWED | Posted: 9 March 2026 doi:10.20944/preprints202510.1554.v7

Galaxy	χ	wRMS(all) [km/s]	wRMS(inner) [km/s]	wRMS(mid) [km/s]	Q $= \mathrm{wRMS}/\langle V_{\mathrm{obs}}\rangle_{\mathrm{outer}}$	Flag	N
NGC5055	0.469	79.9	105.6	81.1	0.449	C	28.
NGC5585	1.640	15.9	16.1	21.1	0.176	B	24.
NGC5907	0.924	20.6	29.4	22.0	0.096	A	19.
NGC5985	1.401	27.6	61.6	11.5	0.095	A	33.
NGC6015	1.208	19.9	14.4	28.2	0.126	B	44.
NGC6503	1.136	17.5	37.8	13.3	0.152	B	31.
NGC6674	1.103	22.1	24.1	27.5	0.092	A	15.
NGC7331	0.359	64.4	134.8	55.5	0.270	C	36.
NGC7793	0.771	12.0	9.5	14.7	0.111	B	46.
NGC7814	0.707	35.2	84.6	32.9	0.164	B	18.
UGC00128	2.278	10.3	15.1	9.6	0.079	A	22.
UGC00191	2.316	7.6	6.9	6.5	0.102	B	9.
UGC01230	2.012	14.8	12.7	20.9	0.139	B	11.
UGC02259	2.880	11.1	26.1	10.3	0.129	B	8.
UGC02487	1.347	9.6	29.0	7.6	0.029	A	17.
UGC02885	0.977	46.5	68.2	47.0	0.156	B	19.
UGC02916	0.345	57.9	81.2	45.8	0.284	C	43.
UGC02953	0.638	52.6	84.9	75.9	0.195	B	115.
UGC03205	0.685	18.0	20.0	33.6	0.083	A	48.
UGC03546	0.366	24.7	111.9	39.3	0.126	B	30.
UGC03580	0.936	39.4	76.6	52.3	0.334	C	47.
UGC04278	2.901	8.3	6.7	11.0	0.095	A	25.
UGC04325	2.845	15.5	22.9	15.6	0.171	B	8.
UGC04483	2.216	0.9	1.7	0.7	0.038	A	8.
UGC04499	2.047	1.6	2.6	1.4	0.023	A	9.
UGC05005	2.314	6.6	5.5	8.9	0.069	A	11.
UGC05253	0.461	56.1	73.4	71.4	0.239	C	73.
UGC05716	2.809	6.2	8.3	6.4	0.084	A	12.
UGC05721	1.940	4.7	6.8	5.0	0.060	A	23.
UGC05750	2.453	4.2	3.9	3.2	0.058	A	11.
UGC05986	1.979	3.6	2.3	4.2	0.032	A	15.
UGC06399	2.631	3.3	3.6	3.6	0.039	A	9.
UGC06446	2.522	9.0	12.3	8.7	0.109	B	17.
UGC06614	0.988	57.8	68.4	66.8	0.287	C	13.
UGC06786	1.001	35.2	60.1	53.4	0.157	B	45.
UGC06787	0.814	60.2	138.6	68.9	0.251	C	71.
UGC06818	1.910	12.1	14.6	13.7	0.186	B	8.
UGC06917	2.006	3.2	3.4	4.1	0.030	A	11.
UGC06930	1.694	4.8	9.0	3.1	0.044	A	10.
UGC06983	2.052	7.8	10.0	7.6	0.072	A	17.
UGC07089	1.590	5.5	5.8	6.1	0.074	A	12.
UGC07125	1.307	2.2	3.3	2.2	0.034	A	13.
UGC07151	1.431	1.7	2.8	1.1	0.023	A	11.
UGC07323	1.288	4.1	5.1	5.4	0.053	A	10.
UGC07524	2.366	4.3	2.0	6.6	0.053	A	31.
UGC07603	2.375	1.8	3.2	1.3	0.030	A	12.
UGC08286	2.574	8.0	14.7	6.6	0.096	A	17.
UGC08490	1.906	2.8	4.5	2.0	0.036	A	30.
UGC08550	2.497	3.4	6.7	0.6	0.061	A	11.
UGC08699	0.620	42.9	63.5	37.1	0.236	C	41.
UGC08837	1.677	4.3	5.2	4.3	0.108	B	8.
UGC09037	0.546	40.8	56.8	24.4	0.270	C	22.

© 2026 by the author(s). Distributed under a Creative Commons CC BY license.

Preprints.org (www.preprints.org) | NOT PEER-REVIEWED | Posted: 9 March 2026 doi:10.20944/preprints202510.1554.v7

Galaxy	χ	wRMS(all) [km/s]	wRMS(inner) [km/s]	wRMS(mid) [km/s]	Q = wRMS/$\langle V_{\rm obs}\rangle_{\rm outer}$	Flag	N
UGC09133	0.719	51.3	124.0	65.5	0.220	C	68.
UGC11820	2.271	1.7	4.3	3.3	0.023	A	10.
UGC12506	1.404	19.7	35.8	10.2	0.085	A	31.
UGC12632	2.673	6.9	10.2	8.2	0.095	A	15.
UGC12732	2.681	5.4	10.4	4.2	0.059	A	16.

Appendix B Comparison of the AT approach to other approaches

Table A2. Benchmark comparison of the weighted RMS residuals for the Alena Tensor constant-χ model (AT) against MOND (with standard a_0) and a one-parameter cored-halo proxy (Burkert-1p), evaluated on the same SPARC rotation-curve points and uncertainties. All wRMS values are computed over the full radial range.

Galaxy	χ	wRMS(AT) [km/s]	wRMS(MOND) [km/s]	wRMS(Burkert-1p) [km/s]	$\langle V_{\rm obs}\rangle_{\rm outer}$ [km/s]	N
D631-7	2.631	7.2	14.8	24.6	57.7	16.
DDO161	2.125	3.1	21.8	11.7	66.3	31.
DDO168	2.640	4.1	10.8	15.2	53.4	10.
DDO170	2.997	5.6	18.3	6.2	59.1	8.
ESO079-G014	1.395	7.1	26.9	20.8	172.6	15.
ESO116-G012	1.931	5.5	8.9	28.0	110.0	15.
ESO563-G021	1.038	32.3	32.9	91.9	314.9	30.
F568-3	2.458	6.7	16.8	51.1	108.5	18.
F568-V1	2.814	19.0	18.0	16.5	113.0	15.
F571-8	1.369	45.8	40.0	61.4	131.8	13.
F574-1	2.319	5.7	10.8	24.6	98.4	14.
F579-V1	1.817	18.6	17.2	15.8	113.4	14.
F583-4	2.062	2.6	16.8	15.8	65.2	12.
IC4202	0.510	41.5	54.8	56.0	242.2	32.
KK98-251	2.822	1.1	12.8	10.9	33.0	15.
NGC0024	1.933	7.2	6.3	22.3	107.0	29.
NGC0055	1.733	3.9	25.8	20.0	86.2	21.
NGC0100	1.983	8.8	18.8	30.3	88.1	21.
NGC0247	2.287	9.2	12.0	34.3	105.7	26.
NGC0289	0.960	31.8	48.6	23.8	167.4	28.
NGC0300	2.267	2.3	9.9	23.9	94.4	25.
NGC1003	1.782	13.0	21.7	21.0	111.4	36.
NGC1090	0.682	16.3	56.7	21.9	162.7	24.
NGC1705	1.906	2.7	8.5	6.5	71.5	14.
NGC2366	1.959	3.8	14.1	14.6	50.1	26.
NGC2403	1.430	17.8	15.3	28.7	133.3	73.
NGC2683	0.475	24.8	52.2	29.9	157.0	11.
NGC2841	1.232	17.8	8.5	28.2	281.8	50.
NGC2903	0.484	51.1	57.4	46.8	182.9	34.
NGC2915	2.100	8.2	15.5	15.7	82.9	30.
NGC2998	0.676	14.1	55.5	14.3	211.2	13.
NGC3198	1.192	22.1	37.9	32.9	148.9	43.
NGC3726	0.700	36.3	70.8	45.5	161.6	12.
NGC3741	2.991	2.6	4.0	17.6	49.5	21.
NGC3769	1.085	26.2	39.9	29.3	117.8	12.
NGC3893	0.570	34.4	48.8	42.4	179.4	10.
NGC3917	1.292	5.1	26.9	26.3	137.2	17.
NGC3972	1.211	5.1	21.6	18.8	127.4	10.

© 2026 by the author(s). Distributed under a Creative Commons CC BY license.

Preprints.org (www.preprints.org) | NOT PEER-REVIEWED | Posted: 9 March 2026 doi:10.20944/preprints202510.1554.v7

Galaxy	χ	wRMS(AT) [km/s]	wRMS(MOND) [km/s]	wRMS(Burkert-1p) [km/s]	$\langle V_{\rm obs} \rangle_{\rm outer}$ [km/s]	N
NGC3992	0.949	9.9	44.3	17.2	245.6	9.
NGC4010	1.031	12.5	33.4	23.7	125.8	12.
NGC4013	0.843	33.0	56.9	43.2	176.9	36.
NGC4100	0.687	12.5	38.4	19.2	165.3	24.
NGC4157	0.447	47.8	75.4	52.2	185.2	17.
NGC4183	1.540	4.6	25.6	15.5	110.8	23.
NGC4214	1.675	8.8	6.7	15.2	80.4	14.
NGC4559	0.938	16.8	42.7	21.7	121.6	32.
NGC5033	0.706	29.1	34.6	20.6	194.2	22.
NGC5055	0.469	79.9	93.4	76.2	178.0	28.
NGC5585	1.640	15.9	19.6	40.4	90.6	24.
NGC5907	0.924	20.6	58.8	26.2	215.8	19.
NGC5985	1.401	27.6	22.3	12.5	291.9	33.
NGC6015	1.208	19.9	24.7	43.5	157.3	44.
NGC6503	1.136	17.5	23.1	15.8	115.2	31.
NGC6674	1.103	22.1	37.8	19.3	241.6	15.
NGC7331	0.359	64.4	93.2	64.4	238.4	36.
NGC7793	0.771	12.0	22.8	26.1	107.6	46.
NGC7814	0.707	35.2	19.5	28.2	214.0	18.
UGC00128	2.278	10.3	16.5	10.7	130.3	22.
UGC00191	2.316	7.6	14.2	13.8	74.1	9.
UGC01230	2.012	14.8	24.0	26.7	106.6	11.
UGC02259	2.880	11.1	4.4	5.9	86.2	8.
UGC02487	1.347	9.6	10.0	13.6	330.8	17.
UGC02885	0.977	46.5	50.4	52.5	298.0	19.
UGC02916	0.345	57.9	65.7	56.2	203.9	43.
UGC02953	0.638	52.6	42.9	48.7	269.7	115.
UGC03205	0.685	18.0	36.5	19.5	217.4	48.
UGC03546	0.366	24.7	52.5	22.3	195.3	30.
UGC03580	0.936	39.4	40.3	39.3	118.2	47.
UGC04278	2.901	8.3	10.7	33.0	86.9	25.
UGC04325	2.845	15.5	8.0	12.9	90.9	8.
UGC04483	2.216	0.9	7.2	4.4	22.6	8.
UGC04499	2.047	1.6	17.5	12.0	71.6	9.
UGC05005	2.314	6.6	25.9	35.5	94.8	11.
UGC05253	0.461	56.1	50.5	52.7	235.1	73.
UGC05716	2.809	6.2	6.4	10.5	73.4	12.
UGC05721	1.940	4.7	10.1	19.1	78.6	23.
UGC05750	2.453	4.2	19.5	29.0	71.9	11.
UGC05986	1.979	3.6	7.6	28.4	111.6	15.
UGC06399	2.631	3.3	9.2	15.8	83.5	9.
UGC06446	2.522	9.0	4.2	12.0	83.1	17.
UGC06614	0.988	57.8	67.4	62.5	201.2	13.
UGC06786	1.001	35.2	14.5	33.8	223.5	45.
UGC06787	0.814	60.2	22.5	44.1	240.0	71.
UGC06818	1.910	12.1	25.2	21.5	64.9	8.
UGC06917	2.006	3.2	15.4	17.3	106.0	11.
UGC06930	1.694	4.8	24.3	12.0	108.0	10.
UGC06983	2.052	7.8	9.2	13.4	108.4	17.
UGC07089	1.590	5.5	28.2	18.6	74.7	12.
UGC07125	1.307	2.2	38.1	8.4	65.3	13.
UGC07151	1.431	1.7	15.5	12.6	72.5	11.

© 2026 by the author(s). Distributed under a Creative Commons CC BY license.

Preprints.org (www.preprints.org) | NOT PEER-REVIEWED | Posted: 9 March 2026 doi:10.20944/preprints202510.1554.v7

Galaxy	χ	wRMS(AT) [km/s]	wRMS(MOND) [km/s]	wRMS(Burkert-1p) [km/s]	$\langle V_{\rm obs} \rangle_{\rm outer}$ [km/s]	N
UGC07323	1.288	4.1	23.8	14.0	78.1	10.
UGC07524	2.366	4.3	15.3	18.8	79.8	31.
UGC07603	2.375	1.8	5.5	16.3	62.0	12.
UGC08286	2.574	8.0	3.4	13.4	83.5	17.
UGC08490	1.906	2.8	1.8	11.4	78.3	30.
UGC08550	2.497	3.4	4.6	10.6	56.2	11.
UGC08699	0.620	42.9	30.6	35.8	181.9	41.
UGC08837	1.677	4.3	21.6	12.1	40.2	8.
UGC09037	0.546	40.8	75.4	48.4	151.3	22.
UGC09133	0.719	51.3	63.2	39.7	232.9	68.
UGC11820	2.271	1.7	16.7	9.4	74.3	10.
UGC12506	1.404	19.7	23.1	13.5	232.3	31.
UGC12632	2.673	6.9	13.7	9.6	72.2	15.
UGC12732	2.681	5.4	10.1	18.0	91.6	16.

© 2026 by the author(s). Distributed under a Creative Commons CC BY license.

Preprints.org (www.preprints.org) | NOT PEER-REVIEWED | Posted: 9 March 2026 doi:10.20944/preprints202510.1554.v7

Appendix C Graphical results of fitting the constant χ

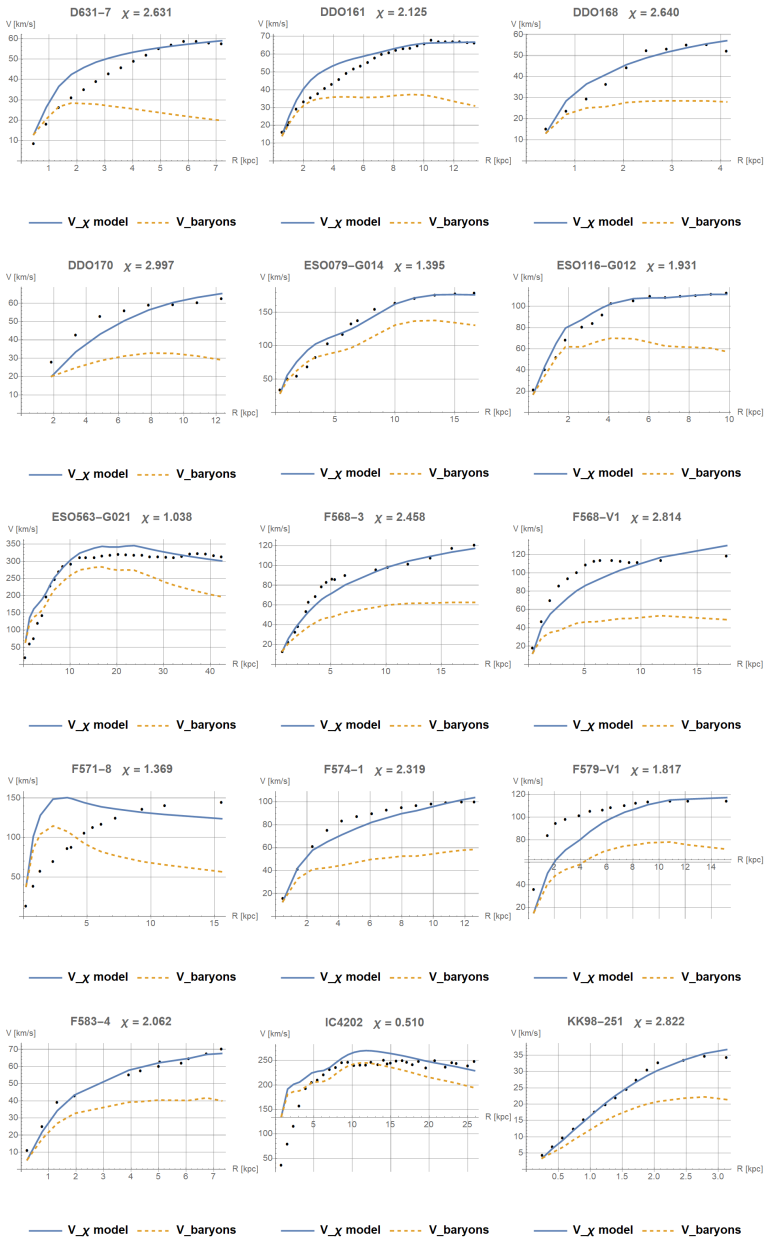

Figure A3. Rotation curves at constant χ for galaxies 1/7

© 2026 by the author(s). Distributed under a Creative Commons CC BY license.

Preprints.org (www.preprints.org) | NOT PEER-REVIEWED | Posted: 9 March 2026 doi:10.20944/preprints202510.1554.v7

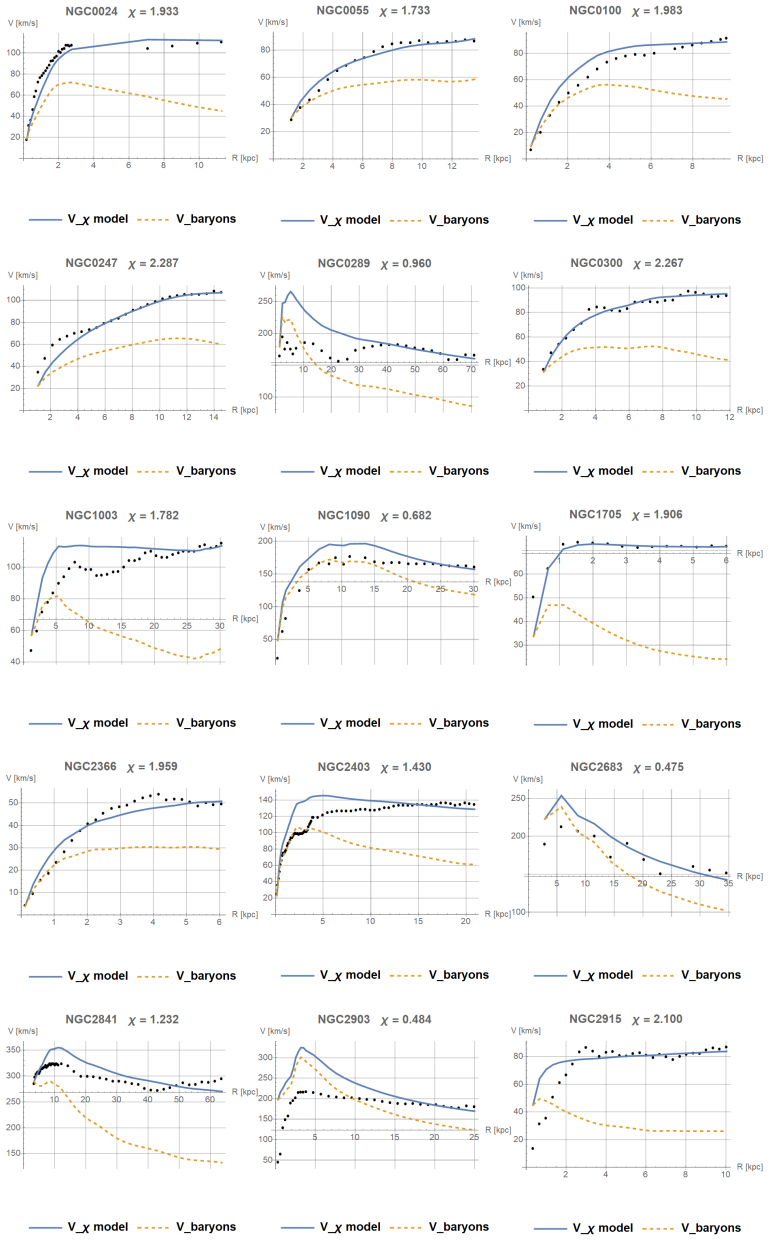

Figure A4. Rotation curves at constant χ for galaxies 2/7

© 2026 by the author(s). Distributed under a Creative Commons CC BY license.

Preprints.org (www.preprints.org) | NOT PEER-REVIEWED | Posted: 9 March 2026 doi:10.20944/preprints202510.1554.v7

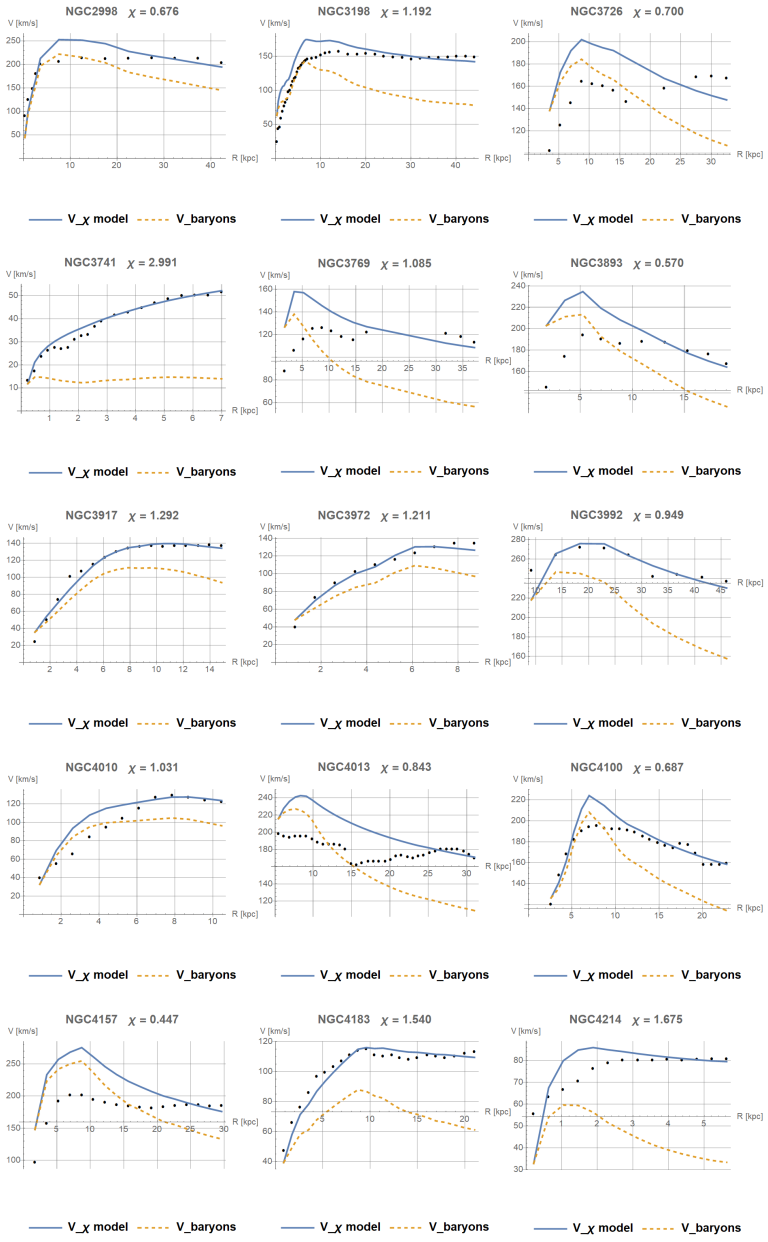

Figure A5. Rotation curves at constant χ for galaxies 3/7

© 2026 by the author(s). Distributed under a Creative Commons CC BY license.

Preprints.org (www.preprints.org) | NOT PEER-REVIEWED | Posted: 9 March 2026 doi:10.20944/preprints202510.1554.v7

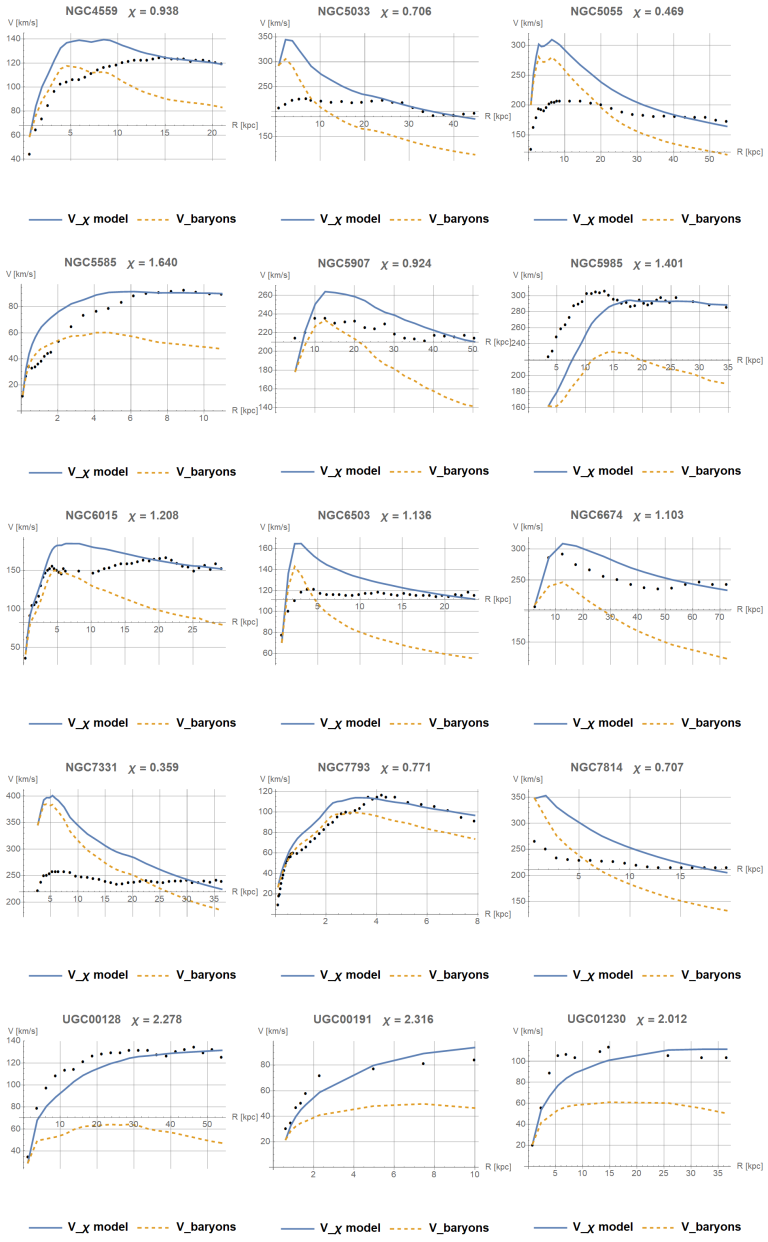

Figure A6. Rotation curves at constant χ for galaxies 4/7

© 2026 by the author(s). Distributed under a Creative Commons CC BY license.

Preprints.org (www.preprints.org) | NOT PEER-REVIEWED | Posted: 9 March 2026 doi:10.20944/preprints202510.1554.v7

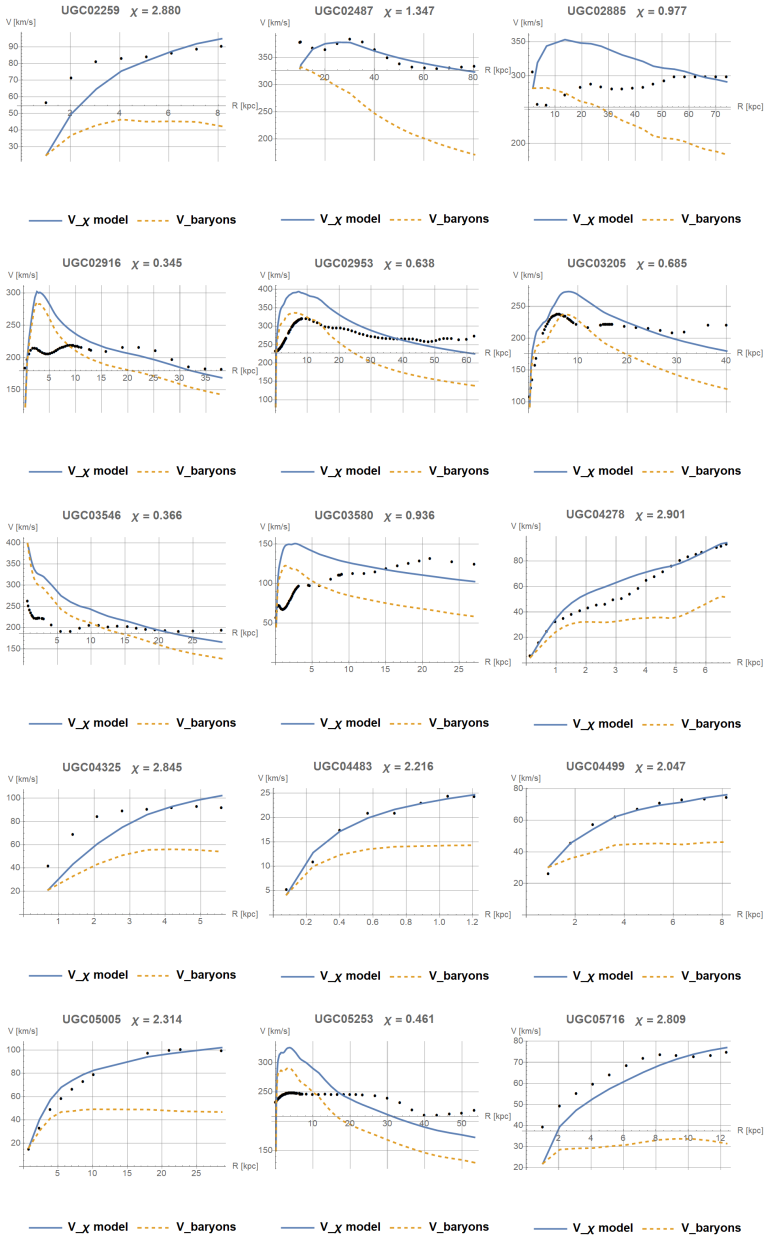

Figure A7. Rotation curves at constant χ for galaxies 5/7

© 2026 by the author(s). Distributed under a Creative Commons CC BY license.

Preprints.org (www.preprints.org) | NOT PEER-REVIEWED | Posted: 9 March 2026 doi:10.20944/preprints202510.1554.v7

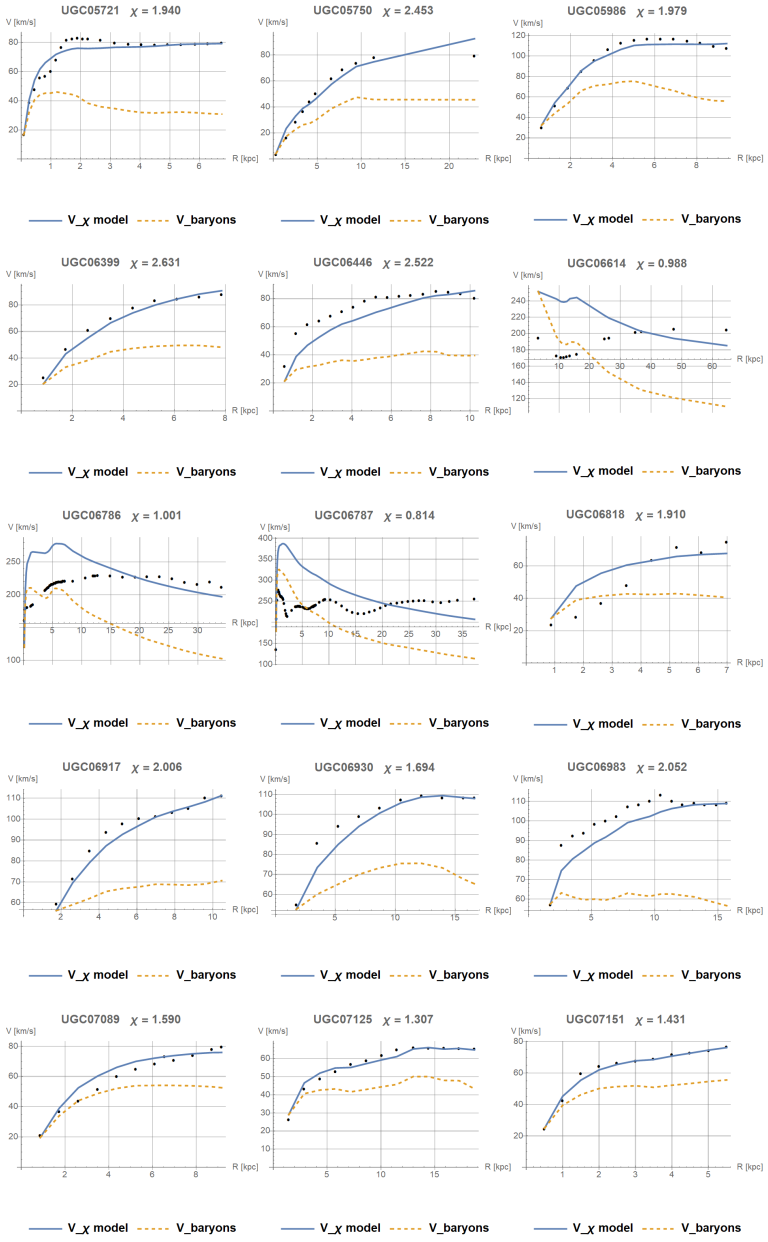

Figure A8. Rotation curves at constant χ for galaxies 6/7

© 2026 by the author(s). Distributed under a Creative Commons CC BY license.

Preprints.org (www.preprints.org) | NOT PEER-REVIEWED | Posted: 9 March 2026 doi:10.20944/preprints202510.1554.v7

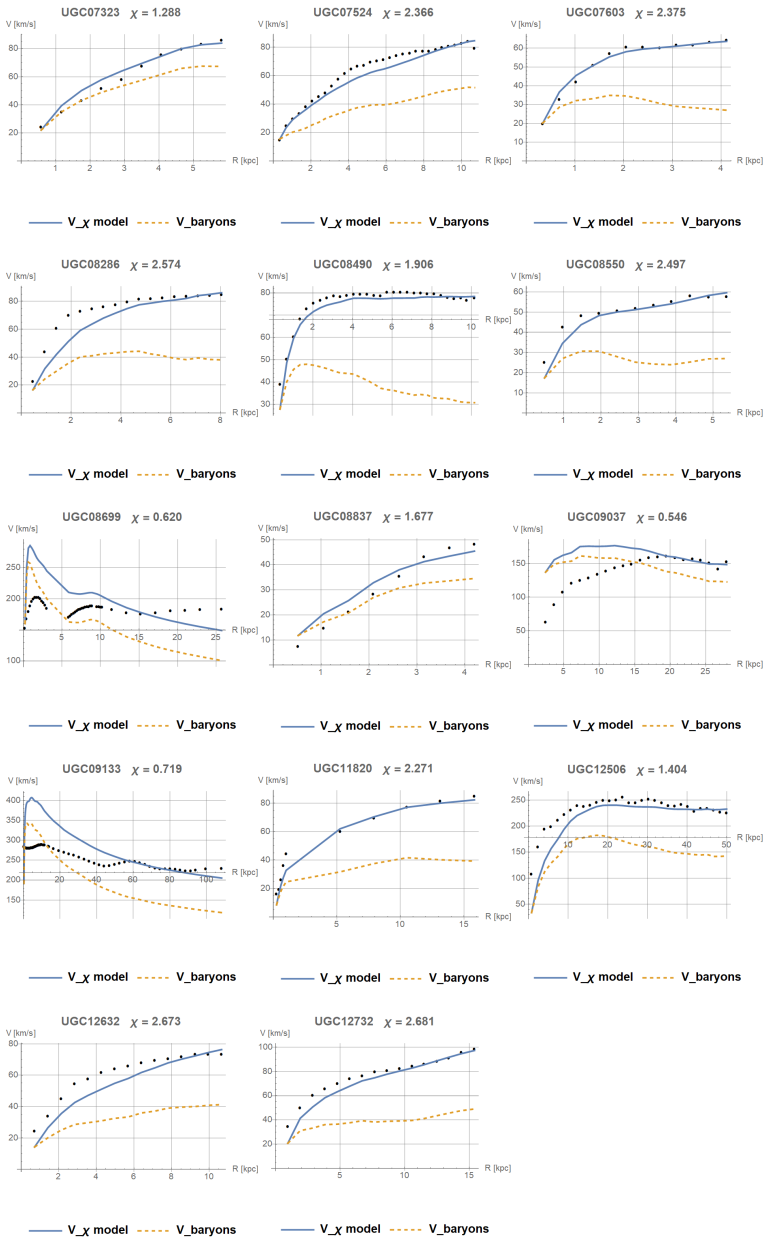

Figure A9. Rotation curves at constant χ for galaxies 7/7

References

1. Abdalla, E.; Marins, A. The dark sector cosmology. *International Journal of Modern Physics D* **2020**, *29*, 2030014. https://doi.org/10.1142/S0218271820300141.
2. Marra, V.; Rosenfeld, R.; Sturani, R. Observing the dark sector. *Universe* **2019**, *5*, 137. https://doi.org/10.3390/universe5060137.
3. Billard, J.; Boulay, M.; Cebrián, S.; Covi, L.; Fiorillo, G.; Green, A.; Kopp, J.; Majorovits, B.; Palladino, K.; Petricca, F.; et al. Direct detection of dark matter-APPEC committee report. *Reports on Progress in Physics* **2022**, *85*, 056201. https://doi.org/10.1088/1361-6633/ac5754.
4. Akerib, D.; Akerlof, C.; Alsum, S.; Araújo, H.; Arthurs, M.; Bai, X.; Bailey, A.; Balajthy, J.; Balashov, S.; Bauer, D.; et al. Projected WIMP sensitivity of the LUX-ZEPLIN dark matter experiment. *Physical Review D* **2020**, *101*, 052002. https://doi.org/10.1103/PhysRevD.101.052002.
5. Nitta, T.; Braine, T.; Du, N.; Guzzetti, M.; Hanretty, C.; Leum, G.; Rosenberg, L.; Rybka, G.; Sinnis, J.; Clarke, J.; et al. Search for a dark-matter-induced cosmic axion background with ADMX. *Physical review letters* **2023**, *131*, 101002. https://doi.org/10.1103/PhysRevLett.131.101002.

© 2026 by the author(s). Distributed under a Creative Commons CC BY license.

Preprints.org (www.preprints.org) | NOT PEER-REVIEWED | Posted: 9 March 2026 doi:10.20944/preprints202510.1554.v7

6. Eckert, D.; Ettori, S.; Robertson, A.; Massey, R.; Pointecouteau, E.; Harvey, D.; McCarthy, I. Constraints on dark matter self-interaction from the internal density profiles of X-COP galaxy clusters. *Astronomy & Astrophysics* **2022**, *666*, A41. https://doi.org/10.1051/0004-6361/202243205.
7. Capolupo, A.; Pisacane, G.; Quaranta, A.; Romeo, F. Probing mirror neutrons and dark matter through cold neutron interferometry. *Physics of the Dark Universe* **2024**, *46*, 101688. https://doi.org/10.1016/j.dark.2024.101688.
8. Aprile, E.; Aalbers, J.; Abe, K.; Ahmed Maouloud, S.; Althueser, L.; Andrieu, B.; Angelino, E.; Antón Martin, D.; Arneodo, F.; Baudis, L.; et al. First search for light dark matter in the neutrino fog with XENONnT. *Physical Review Letters* **2025**, *134*, 111802. https://doi.org/10.1103/PhysRevLett.134.111802.
9. Agnese, R.; Aralis, T.; Aramaki, T.; Arnquist, I.; Azadbakht, E.; Baker, W.; Banik, S.; Barker, D.; Bauer, D.; Binder, T.; et al. First dark matter constraints from a SuperCDMS single-charge sensitive detector. *Physical review letters* **2018**, *121*, 051301. https://doi.org/10.1103/PhysRevLett.121.051301.
10. Kamionkowski, M.; Riess, A.G. The Hubble Tension and Early Dark Energy. *Annual Review of Nuclear and Particle Science* **2023**, *73*, 153–180. https://doi.org/10.1146/annurev-nucl-111422-024107.
11. Aghanim, N.; et al. Planck 2018 results. VI. Cosmological parameters. *Astronomy & Astrophysics* **2020**, *641*, A6. https://doi.org/10.1051/0004-6361/201833910.
12. Skordis, C.; Złośnik, T. New Relativistic Theory for Modified Newtonian Dynamics. *Physical Review Letters* **2021**, *127*, 161302. https://doi.org/10.1103/PhysRevLett.127.161302.
13. Nash, G. Modified general relativity and dark matter. *International Journal of Modern Physics D* **2023**, *32*, 2350031. https://doi.org/10.1142/S0218271823500311.
14. Andreev, Y.M.; Banerjee, D.; Banto Oberhauser, B.; Bernhard, J.; Bisio, P.; Celentano, A.; Charitonidis, N.; Chumakov, A.; Cooke, D.; Crivelli, P.; et al. Search for light dark matter with NA64 at CERN. *Physical Review Letters* **2023**, *131*, 161801. https://doi.org/10.1103/PhysRevLett.131.161801.
15. Ishak, M. Testing general relativity in cosmology. *Living Reviews in Relativity* **2019**, *22*, 1. https://doi.org/10.1007/s41114-018-0017-4.
16. Anchordoqui, L.A.; Antoniadis, I.; Lüst, D.; Castillo, K.P. Through the looking glass into the dark dimension: Searching for bulk black hole dark matter with microlensing of X-ray pulsars. *Physics of the Dark Universe* **2024**, *46*, 101681. https://doi.org/10.1016/j.dark.2024.101681.
17. Brouwer, M.; et al. First test of Verlinde's theory of emergent gravity using weak gravitational lensing measurements. *Monthly Notices of the Royal Astronomical Society* **2017**, *466*, 2547–2559. https://doi.org/10.1093/mnras/stw3192.
18. Aprile, E.; et al. First Dark Matter Search Results from the XENON1T Experiment. *Phys. Rev. Lett.* **2017**, *119*, 181301. https://doi.org/10.1103/PhysRevLett.119.181301.
19. Khoury, J. Dark Matter Superfluidity. *SciPost Physics Lecture Notes* **2022**, *42*. https://doi.org/10.21468/SciPostPhysLectNotes.42.
20. Goddy, J.; et al. A comparison of the baryonic Tully-Fisher relation in MaNGA and SPARC. *Monthly Notices of the Royal Astronomical Society* **2023**, *520*, 3895–3912. https://doi.org/10.1093/mnras/stad298.
21. Lucca, M. Dark energy-dark matter interactions as a solution to the S_8 tension. *Physics of the Dark Universe* **2021**, *34*, 100899. https://doi.org/10.1016/j.dark.2021.100899.
22. Brout, D.; others (Pantheon+ Collaboration). The Pantheon+ Analysis: Cosmological Constraints. *The Astrophysical Journal* **2022**, *938*, 110. https://doi.org/10.3847/1538-4357/ac8e04.
23. Lodha, K.; et al. DESI 2024: Constraints on physics-focused aspects of dark energy using DESI DR1 BAO data. *Phys. Rev. D* **2025**, *111*, 023532. https://doi.org/10.1103/PhysRevD.111.023532.
24. Cuillandre, J.C.; others (Euclid Collaboration). Euclid: Early Release Observations - Programme overview and data products. *Astronomy & Astrophysics* **2025**, *686*, A1. https://doi.org/10.1051/0004-6361/202450803.
25. Ogonowski, P. Proposed method of combining continuum mechanics with Einstein Field Equations. *International Journal of Modern Physics D* **2023**, *2350010*, 15. https://doi.org/10.1142/S0218271823500104.
26. Ogonowski, P. Developed method: interactions and their quantum picture. *Frontiers in Physics* **2023**, *11:1264925*. https://doi.org/10.3389/fphy.2023.1264925.
27. Ogonowski, P. Gravitational waves and Higgs-like potential from Alena Tensor. *Physica Scripta* **2025**, *100*. https://doi.org/10.1088/1402-4896/ae12e2.
28. Ogonowski, P.; Skindzier, P. Alena Tensor in unification applications. *Physica Scripta* **2024**, *100*, 015018. https://doi.org/10.1088/1402-4896/ad98ca.
29. Forger, M.; Römer, H. Currents and the energy-momentum tensor in classical field theory: a fresh look at an old problem. *Annals of Physics* **2004**, *309*, 306–389. https://doi.org/10.1016/j.aop.2003.08.011.

© 2026 by the author(s). Distributed under a Creative Commons CC BY license.

Preprints.org (www.preprints.org) | NOT PEER-REVIEWED | Posted: 9 March 2026 doi:10.20944/preprints202510.1554.v7

30. Blaschke, D.N.; Gieres, F.; Reboud, M.; Schweda, M. The energy-momentum tensor(s) in classical gauge theories. *Nuclear Physics B* **2016**, *912*, 192–223. https://doi.org/10.1016/j.nuclphysb.2016.07.001.
31. Vossos, S.; Vossos, E.; Ntelis, C. The Equations of Motion in Spacetime endowed with Stationary metric of General Relativity and the equivalent Gravitational Scalar Generalized Potential of Special Relativity. *Classical and Quantum Gravity* **2026**. https://doi.org/10.1088/1361-6382/ae4202.
32. Bardeen, J.M.; Press, W.H.; Teukolsky, S.A. Rotating Black Holes: Locally Nonrotating Frames, Energy Extraction, and Scalar Synchrotron Radiation. *The Astrophysical Journal* **1972**, *178*, 347–370. https://doi.org/10.1086/151796.
33. Abramowicz, M.A.; Jaroszynski, M.; Sikora, M. Relativistic, accreting disks. *Astronomy and Astrophysics* **1978**, *63*, 221–224.
34. Abramowicz, M.A.; Fragile, P.C. Foundations of Black Hole Accretion Disk Theory. *Living Reviews in Relativity* **2013**, *16*, 1. https://doi.org/10.12942/lrr-2013-1.
35. Lelli, F.; McGaugh, S.S.; Schombert, J.M. SPARC: Mass Models for 175 Disk Galaxies with Spitzer Photometry and Accurate Rotation Curves. *The Astronomical Journal* **2016**, *152*, 157. https://doi.org/10.3847/0004-6256/152/6/157.
36. Stewart, K.R.; Brooks, A.M.; Bullock, J.S.; Maller, A.H.; Diemand, J.; Wadsley, J.; Moustakas, L.A. Angular momentum acquisition in galaxy halos. *The Astrophysical Journal* **2013**, *769*, 74. https://doi.org/10.1088/0004-637X/769/1/74.
37. Stewart, K.R.; Maller, A.H.; Oñorbe, J.; Bullock, J.S.; Joung, M.R.; Devriendt, J.; Ceverino, D.; Kereš, D.; Hopkins, P.F.; Faucher-Giguère, C.A. High angular momentum halo gas: a feedback and code-independent prediction of LCDM. *The Astrophysical Journal* **2017**, *843*, 47. https://doi.org/10.3847/1538-4357/aa6dff.
38. Mancera Piña, P.E.; Fraternali, F.; Oosterloo, T.; Adams, E.A.; Teodoro, E.d.; Bacchini, C.; Iorio, G. The impact of gas disc flaring on rotation curve decomposition and revisiting baryonic and dark matter relations for nearby galaxies. *Monthly Notices of the Royal Astronomical Society* **2022**, *514*, 3329–3348. https://doi.org/10.1093/mnras/stac1508.
39. Bartelmann, M.; Schneider, P. Weak gravitational lensing. *Reports on Progress in Physics* **2001**, *64*, 691–757. https://doi.org/10.1016/S0370-1573(00)00082-X.
40. Koyama, K. Cosmological tests of modified gravity. *Reports on Progress in Physics* **2016**, *79*, 046902. https://doi.org/10.1088/0034-4885/79/4/046902.
41. Harvey-Hawes, C.; Galoppo, M. A Novel Test for MOND: Gravitational Lensing by Disk Galaxies. *The Astrophysical Journal* **2025**, *994*, 167. https://doi.org/10.3847/1538-4357/ae11ad.
42. Best, H.; Fagin, J.; Vernardos, G.; O'Dowd, M. Resolving the vicinity of supermassive black holes with gravitational microlensing. *Monthly Notices of the Royal Astronomical Society* **2024**, *531*, 1095–1112. https://doi.org/10.1093/mnras/stae1182.
43. Vernardos, G.; Sluse, D.; Pooley, D.; Schmidt, R.W.; Millon, M.; Weisenbach, L.; Motta, V.; Anguita, T.; Saha, P.; O'Dowd, M.; et al. Microlensing of Strongly Lensed Quasars. *Space Science Reviews* **2024**, *220*, 14. https://doi.org/10.1007/s11214-024-01043-8.
44. Román-Roche, J.; Herráiz-López, V.; Zueco, D. Exact solution for quantum strong long-range models via a generalized Hubbard-Stratonovich transformation. *Physical Review B* **2023**, *108*, 165130. https://doi.org/10.1103/PhysRevB.108.165130.
45. Cacciapaglia, G.; Frandsen, M.T.; Huang, W.C.; Rosenlyst, M.; Sørensen, P. Techni-composite Higgs models with symmetric and asymmetric dark matter candidates. *Physical Review D* **2022**, *106*, 075022. https://doi.org/10.1103/PhysRevD.106.075022.
46. Del Debbio, L.; Zwicky, R. Dilaton and massive hadrons in a conformal phase. *Journal of High Energy Physics* **2022**, *2022*, 1–21. https://doi.org/10.1007/JHEP08(2022)007.
47. Oevermann, E.; Koenigstein, A.; Floerchinger, S. Functional renormalization of QCD in 1+ 1 dimensions: Four-fermion interactions from quark-gluon dynamics. *Physical Review D* **2025**, *111*, 074006. https://doi.org/10.1103/PhysRevD.111.074006.
48. Wang, Y.; Matsuzaki, S.; Kawaguchi, M.; Tomiya, A. First-order CP phase transition in two-flavor QCD at $\theta = \pi$ under electromagnetic scale anomaly via a Nambu-Jona-Lasinio description. *Physical Review D* **2025**, *111*, 074028. https://doi.org/10.1103/PhysRevD.111.074028.
49. Gudnason, S.B.; Speight, J.M. Backreacted Coulomb energy in the Skyrme model. *Journal of High Energy Physics* **2025**, *2025*, 1–59. https://doi.org/10.1007/JHEP01(2025)150.
50. Gudnason, S.B.; Halcrow, C. Quantum binding energies in the Skyrme model. *Physics Letters B* **2024**, *850*, 138526. https://doi.org/10.1016/j.physletb.2024.138526.

© 2026 by the author(s). Distributed under a Creative Commons CC BY license.

Preprints.org (www.preprints.org) | NOT PEER-REVIEWED | Posted: 9 March 2026 doi:10.20944/preprints202510.1554.v7

51. Naya, C.; Schubring, D.; Shifman, M.; Wang, Z. Skyrmions and hopfions in three-dimensional frustrated magnets. *Physical Review B* **2022**, *106*, 094434. https://doi.org/10.1103/PhysRevB.106.094434.
52. Shen, Y.; He, C.; Song, Z.; Chen, B.; He, H.; Ma, Y.; Fells, J.A.; Elston, S.J.; Morris, S.M.; Booth, M.J.; et al. Topologically controlled multiskyrmions in photonic gradient-index lenses. *Physical Review Applied* **2024**, *21*, 024025. https://doi.org/10.1103/PhysRevApplied.21.024025.
53. Volovik, G.E. *The Universe in a Helium Droplet*; Oxford University Press, 2003.
54. Annala, T.; Zamora-Zamora, R.; Möttönen, M. Topologically protected vortex knots and links. *Communications Physics* **2022**, *5*, 309. https://doi.org/10.1038/s42005-022-01071-2.
55. Mashhoon, B.; Obukhov, Y.N. Spin-of-light gyroscope and the spin-rotation coupling. *Physical Review D* **2024**, *110*, 104015. https://doi.org/10.1103/PhysRevD.110.104015.
56. Hehl, F.W.; Ni, W.T. Inertial effects of a Dirac particle. *Phys. Rev. D* **1990**, *42*, 2045–2048. https://doi.org/10.1103/PhysRevD.42.2045.
57. Obukhov, Y.N.; Silenko, A.J.; Teryaev, O.V. Manifestations of the rotation and gravity of the Earth in high-energy physics experiments. *Physical Review D* **2016**, *94*, 044019. https://doi.org/10.1103/PhysRevD.94.044019.
58. Cong, L.; Ji, W.; Fadeev, P.; Ficek, F.; Jiang, M.; Flambaum, V.V.; Guan, H.; Jackson Kimball, D.F.; Kozlov, M.G.; Stadnik, Y.V.; et al. Spin-dependent exotic interactions. *Rev. Mod. Phys.* **2025**, *97*, 025005. https://doi.org/10.1103/RevModPhys.97.025005.
59. Danner, A.; Demirel, B.; Kersten, W.; Lemmel, H.; Wagner, R.; Sponar, S.; Hasegawa, Y. Spin-rotation coupling observed in neutron interferometry. *npj Quantum Information* **2020**, *6*, 23. https://doi.org/10.1038/s41534-020-0254-8.
60. Jiang, L.; Liu, J.; Liang, Y.; Tian, M.; Quan, W. A single-beam dual-axis atomic spin comagnetometer for rotation sensing. *Applied Physics Letters* **2022**, *120*. https://doi.org/10.1063/5.0079429.
61. Huang, X.; Wei, K.; Rui, Y.; Gong, D.; Zhou, S.; Zheng, J.; Quan, W. Dynamically polarized atomic comagnetometer. *Cell Reports Physical Science* **2025**, *6*. https://doi.org/10.1016/j.xcrp.2025.102961.
62. et al., T.E.C. Strong Gravitational Lensing as a Probe of Dark Matter. *Space Science Reviews* **2024**, *220*, 87. https://doi.org/10.1007/s11214-024-01087-w.
63. Cadoni, M.; Sanna, A.P.; Tuveri, M. Anisotropic fluid cosmology: an alternative to dark matter? *Physical Review D* **2020**, *102*, 023514. https://doi.org/10.1103/PhysRevD.102.023514.
64. Cadoni, M.; Casadio, R. Effective fluid description of the dark universe. *Physics Letters B* **2018**, *776*, 242–248. https://doi.org/10.1016/j.physletb.2017.11.058.
65. et al., B.D. Anisotropic strong lensing as a probe of dark matter self-interaction. *Monthly Notices of the Royal Astronomical Society* **2023**, *526*, 5455–5473. https://doi.org/10.1093/mnras/stad3099.
66. et al., D.P. Dark matter fluid constraints from galaxy rotation curves. *European Physical Journal C* **2023**, *83*, 11457. https://doi.org/10.1140/epjc/s10052-023-11457-3.
67. Kuncewicz, J. Perfect fluid dark matter: a viability test with galaxy rotation curves. *The European Physical Journal C* **2025**, *85*, 979. https://doi.org/10.1140/epjc/s10052-025-14705-w.
68. Jusufi, K.; Sheykhi, A.; Capozziello, S. Apparent dark matter as a non-local manifestation of emergent gravity. *Physics of the Dark Universe* **2023**, *42*, 101270. https://doi.org/10.1016/j.dark.2023.101270.
69. Perković, D.; Štefančić, H. Dark matter fluid constraints from galaxy rotation curves. *European Physical Journal C* **2023**, *83*, 306. https://doi.org/10.1140/epjc/s10052-023-11457-3.
70. Rourke, C. A geometric alternative to dark matter, 2020, [arXiv:physics.gen-ph/1911.08920]. https://doi.org/10.48550/arXiv.1911.08920.
71. Konno, K.; Matsuyama, T.; Asano, Y.; Tanda, S. Flat rotation curves in Chern-Simons modified gravity. *Physical Review D* **2008**, *78*, 024037. https://doi.org/10.1103/PhysRevD.78.024037.
72. Balasin, H.; Grumiller, D. Non-Newtonian behavior in weak field general relativity for extended rotating sources. *International Journal of Modern Physics D* **2008**, *17*, 475–488. https://doi.org/10.1142/S0218271808012140.
73. Hanafy, W.E.; Hashim, M.; Nashed, G.G.L. Revisiting flat rotation curves in Chern-Simons modified gravity. *Physics Letters B* **2024**, *856*, 138882. https://doi.org/10.1016/j.physletb.2024.138882.
74. Walrand, S. A machian model as potential alternative to dark matter halo thesis in galactic rotational velocity prediction. *Frontiers in Astronomy and Space Sciences* **2024**, *11*, 1429235. https://doi.org/10.3389/fspas.2024.1429235.
75. Hossenfelder, S. Covariant version of Verlinde's emergent gravity. *Physical Review D* **2017**, *95*, 124018. https://doi.org/10.1103/PhysRevD.95.124018.

© 2026 by the author(s). Distributed under a Creative Commons CC BY license.

Preprints.org (www.preprints.org) | NOT PEER-REVIEWED | Posted: 9 March 2026 doi:10.20944/preprints202510.1554.v7

76. Czuchry, E. Resolution of Cosmological Singularity in Hořava-Lifshitz Cosmology. *Universe* **2023**, *9*, 160. https://doi.org/10.3390/universe9040160.
77. Acquaviva, G.; et al. Simple-graduated dark energy and spatial curvature. *Physical Review D* **2021**, *104*, 023505. https://doi.org/10.1103/PhysRevD.104.023505.
78. Buchert, T.; Räsänen, S. Backreaction in Late-Time Cosmology. *Annual Review of Nuclear and Particle Science* **2012**, *62*, 57–79. https://doi.org/10.1146/annurev.nucl.012809.104435.
79. Gao, D.; Zhou, L.; Wang, J.; Zhan, M. Constraining the spin-gravity coupling effects to the 10- 10 level with dual-species atom interferometers. *Physical Review A* **2024**, *110*, 043322. https://doi.org/10.1103/PhysRevA.110.043322.
80. Obukhov, Y.N. Spin, Gravity, and Inertia. *Phys. Rev. Lett.* **2001**, *86*, 192–195. https://doi.org/10.1103/PhysRevLett.86.192.
81. Silenko, A.J. Foldy-Wouthuysen Transformation and Semiclassical Limit for Relativistic Particles. *Phys. Rev. A* **2005**, *72*, 012118. https://doi.org/10.1103/PhysRevA.77.012116.
82. Becattini, F.; Lisa, M.A. Polarization and vorticity in the quark–gluon plasma. *Annual Review of Nuclear and Particle Science* **2020**, *70*, 395–423. https://doi.org/10.1146/annurev-nucl-021920-095245.
83. Tatara, G. Hydrodynamic theory of vorticity-induced spin transport. *Physical Review B* **2021**, *104*, 184414. https://doi.org/10.1103/PhysRevB.104.184414.
84. Singh, S.K.; Alam, J. Suppression of spin polarization as an indicator of QCD critical point. *The European Physical Journal C* **2023**, *83*, 585. https://doi.org/10.1140/epjc/s10052-023-11776-5.
85. Huidobro, M.; Leask, P.; Naya, C.; Wereszczyński, A. Compressibility of dense nuclear matter in the ρ-meson variant of the Skyrme model. *Journal of High Energy Physics* **2025**, *2025*, 1–25. https://doi.org/10.1007/JHEP01(2025)048.
86. Saavedra, E.; Altbir, D.; Escrig, J.; Castillo-Sepúlveda, S.; Corona, R.; Carvalho-Santos, V. Exploring hopfion stability and dynamics in ring-like structures. *Results in Physics* **2024**, *62*, 107835. https://doi.org/10.1016/j.rinp.2024.107835.
87. Battye, R.A.; Sutcliffe, P.M. Solitons, links and knots. *Proceedings of the Royal Society of London. Series A: Mathematical, Physical and Engineering Sciences* **1999**, *455*, 4305–4331. https://doi.org/10.1098/rspa.1999.0502.
88. Nitta, M. Relations among topological solitons. *Physical Review D* **2022**, *105*, 105006. https://doi.org/10.1103/PhysRevD.105.105006.
89. Cao, G. Extended Nambu-Jona-Lasinio model for quark and nuclear matters. *Physics Letters B* **2025**, *860*, 139140. https://doi.org/10.1016/j.physletb.2024.139140.
90. Covone, S.; Davighi, J.; Isidori, G.; Pesut, M.; et al. Flavour deconstructing the composite Higgs. *Journal of High Energy Physics* **2025**, p. 041. https://doi.org/10.1007/JHEP01(2025)041.
91. Carragher, E.; et al. Extending global fits of 4D composite Higgs models with partially composite leptons. *Journal of High Energy Physics* **2024**, p. 185. https://doi.org/10.1007/JHEP08(2024)185.
92. Zajc, W.A. The fluid nature of quark-gluon plasma. *Nuclear Physics A* **2008**, *805*, 283c–294c. https://doi.org/10.1016/j.nuclphysa.2008.02.285.
93. Barraco, D.E.; Hamity, V.H.; Gleiser, R.J. Anisotropic spheres in general relativity reexamined. *Physical Review D* **2003**, *67*, 064003. https://doi.org/10.1103/PhysRevD.67.064003.
94. Lopes, L.L. Role of local anisotropy in hybrid stars. *The European Physical Journal C* **2024**, *84*, 13442. https://doi.org/10.1140/epjc/s10052-024-13442-w.
95. Son, D.T.; Surówka, P. Hydrodynamics with Triangle Anomalies. *Phys. Rev. Lett.* **2009**, *103*, 191601. https://doi.org/10.1103/PhysRevLett.103.191601.
96. Lin, S.; Yang, L. Magneto-vortical effect in strong magnetic field. *Journal of High Energy Physics* **2021**, *2021*, 1–28. https://doi.org/10.1007/JHEP06(2021)054.
97. Brax, P.; Fichet, S. Scalar-mediated quantum forces between macroscopic bodies and interferometry. *Physics of the Dark Universe* **2023**, *42*, 101294. https://doi.org/10.1016/j.dark.2023.101294.
98. Malaver, M.; Assunção, A.K.T.; Moraes, P.H.R.S. Realistic anisotropic neutron stars: Pressure effects. *Physical Review D* **2024**, *109*, 043025. https://doi.org/10.1103/PhysRevD.109.043025.
99. Lopes, L.L.; Das, H. Spherically symmetric anisotropic strange stars. *The European Physical Journal C* **2024**, *84*, 166. https://doi.org/10.1140/epjc/s10052-024-12520-3.
100. Yau, H. Quantized field with excitations of spacetime. *Scientific Reports* **2025**, *15*, 30844. https://doi.org/10.1038/s41598-025-16139-6.

© 2026 by the author(s). Distributed under a Creative Commons CC BY license.

Preprints.org (www.preprints.org) | NOT PEER-REVIEWED | Posted: 9 March 2026 doi:10.20944/preprints202510.1554.v7

Disclaimer/Publisher's Note: The statements, opinions and data contained in all publications are solely those of the individual author(s) and contributor(s) and not of MDPI and/or the editor(s). MDPI and/or the editor(s) disclaim responsibility for any injury to people or property resulting from any ideas, methods, instructions or products referred to in the content.

© 2026 by the author(s). Distributed under a Creative Commons CC BY license.